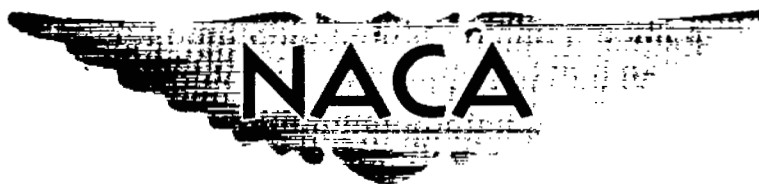


~~CONFIDENTIAL~~

5
Copy
RM E56L11

C.1

NACA RM E56L11



RESEARCH MEMORANDUM

CLASSIFICATION CHANGED

UNCLASSIFIED

Authority of **INVESTIGATION OF AN UNDERSLUNG SCOOP INLET AT**

NASA Class. Change **MACH NUMBERS TO 1.99**

Notices No. 19 dttd May 26, 1965.

By Maynard I. Weinstein, Donald J. Vargo, and Frank McKevitt

MAR-7-1-65

Lewis Flight Propulsion Laboratory
Cleveland, Ohio

LIBRARY COPY

MAR 21 1957

LANGLEY AERONAUTICAL LABORATORY
LIBRARY, NACA
LANGLEY FIELD, VIRGINIA

CLASSIFIED DOCUMENT

This material contains information affecting the National Defense of the United States within the meaning of the espionage laws, Title 18, U.S.C., Secs. 793 and 794, the transmission or revelation of which in any manner to an unauthorized person is prohibited by law.

**NATIONAL ADVISORY COMMITTEE
FOR AERONAUTICS**

WASHINGTON

March 13, 1957

~~CONFIDENTIAL~~

UNCLASSIFIED

UNCLASSIFIED



3 1176 01436 5572

NATIONAL ADVISORY COMMITTEE FOR AERONAUTICS

RESEARCH MEMORANDUM

INVESTIGATION OF AN UNDERSLUNG SCOOP INLET AT MACH NUMBERS TO 1.99

By Maynard I. Weinstein, Donald J. Vargo, and Frank McKevitt

SUMMARY

The performance of a scoop-type inlet on the bottom of a body of revolution was studied at Mach numbers of 0.63 and 1.50 to 1.99 and at angles of attack to 10° . Semielliptic in its frontal projection, the inlet was designed for two-dimensional compression; a compression angle of 14.2° relative to the body centerline provided shock-on-lip operation at Mach number 2.00. The investigation included a study of the effects of altering the approach surface ahead of the inlet, extending the boundary-layer splitter plate, and bleeding air at the throat and exit of the diffuser.

Peak total-pressure recoveries were 0.93, 0.875, and 0.78 at zero angle of attack at Mach numbers of 1.50, 1.79, and 1.99, respectively, for the configuration having a 2.22° inward turning of the body flat ahead of the inlet. With a body flat parallel to the fuselage centerline, pressure recoveries were increased to 0.80. Bleeding air from either flush slots or ram scoops at the inlet throat increased the peak pressure recovery to about 0.83 at Mach number 1.99.

Subcritical flow instabilities, found primarily at Mach number 1.99, were caused by interaction of the terminal shock with the boundary layer of either the splitter plate or the fuselage and consequent separation of the boundary layer. Severe pressure fluctuations encountered with separation of the fuselage boundary layer would preclude operation under such conditions. Increasing the length of the boundary-layer splitter plate considerably improved the stable range, as did the use of the body flat parallel to the fuselage centerline. Stability was decreased with the use of flush bleed slots. The maximum stability obtained at Mach number 1.99 was on the order of 20 percent of critical mass flow.

INTRODUCTION

The NACA Lewis laboratory has investigated a supersonic scoop-type inlet-forebody combination of a proposed missile. The inlet was approximately semielliptic in its projected frontal shape, with a height-to-maximum-width ratio of about 0.83. Although the compression surface was

UNCLASSIFIED

not planar, the scoop was designed for two-dimensional supersonic compression with a design Mach number of 2.00.

Previous investigations of the scoop-type inlet have pointed out such problems as (1) the need for fuselage boundary-layer removal (refs. 1 to 4), (2) the difficulties in starting the inlet flow (ref. 1 and section G of ref. 5), and (3) the tendency for unstable subcritical flow (ref. 3). Ferri in reference 5 proposed a variable-geometry technique and the use of a precompression bump to improve pressure recovery, to aid the starting problem, and to help remove boundary layer. Although these first scoop inlets were rectangular, tests have been made of the structurally more desirable rounded cowls. For example, reference 6 describes the design and testing of a two-dimensional and a three-dimensional compression scoop, each with a semicircular cowl.

The inlets cited were not tested in the flow field of an actual fuselage, nor did the cross sections and turnings of the subsonic diffusers simulate those appropriate to actual installations. These effects are included in the present study. In addition, this investigation determined the effect on inlet performance of alternate fuselage flats ahead of the inlet, of various lengths and heights of the boundary-layer splitter plate, and of bleed at the throat and exit of the diffuser. Data were obtained at Mach numbers 0.63 and 1.50 to 1.99 at a Reynolds number of approximately 25×10^6 based on body length ahead of the inlet.

SYMBOLS

A	area
A_c	inlet capture area projected on a plane perpendicular to approach A, 0.131 sq ft
A_F	model frontal area, 0.905 sq ft
A_2	flow area at diffuser exit, 0.158 sq ft
C_D	drag coefficient based on A_F
h	splitter height
M	Mach number
m_2/m_0	mass-flow ratio, $\frac{\rho_2 V_2 A_2}{\rho_0 V_0 A_c}$
P	total pressure

ΔP difference between maximum and minimum total pressures at diffuser-exit rake

$\Delta P/P_2$ distortion parameter

P' Pitot pressure

p static pressure

V velocity

y distance from fuselage, in.

α angle of attack, deg

δ boundary-layer thickness, in.

ρ density

Subscripts:

f fuselage survey station

max maximum

0 free stream

1 inlet throat station

2 diffuser-exit station

APPARATUS AND PROCEDURE

General Model Description

The test configuration was essentially a 1/5-scale forebody of a supersonic missile (figs. 1 and 2). The underslung, scoop-type inlet was mounted approximately 6 body diameters aft of the nose. Except for a flattened approach surface, the fuselage ahead of the inlet consisted of a body of revolution with a maximum diameter of 10 inches. An offset in the support sting was required to allow the duct flow to discharge on the model centerline as in the actual missile. (Fuselage lines were thus altered to fair over this offset.) A sting-mounted, sheet-metal shroud extending the model lines aft of the base was used to promote uniform base pressures. Forces were measured with a two-component internal strain-gage balance and a lift link at the base of the model. Mass flow was controlled with a remotely actuated plug supported from the sting.

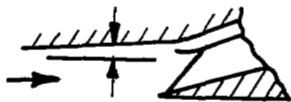
Details of the inlet are shown in figure 3. Approximately semi-elliptical in its projected area shape, the inlet had a height-to-maximum-width ratio of about 0.83. The inlet was designed for two-dimensional supersonic compression; the compression surface was essentially held at a constant angle in pitch planes across its width (14.2° with respect to the fuselage centerline). The lip was sharp and was swept back at 43.75° so as to very nearly coincide with the oblique-shock angle at Mach number 2.00.

Fuselage Boundary-Layer Removal

Boundary layer was removed ahead of the inlet by a splitter-diverter system. Two boundary-layer splitter plates (sketched in fig. 3) were tested. The splitter designated "long" extended 0.8 inch forward of the one designated "short." The internal-flow surface of each splitter was faired upward from the leading edge rather than extended directly rearward to the throat; the penalty of a supersonic expansion ahead of the throat was thus introduced in order to provide a larger throat area for more efficient engine matching at the subsonic cruising speed. Area distribution through the subsonic diffuser is shown in figure 4.

The fuselage boundary layer removed by the splitter was directed upward through a channel of gradually increasing height and outward by a centrally located diverter (fig. 5(a)). The effect of enclosing the boundary-layer channel with side plates was briefly examined. These enclosed passages, designated "long duct" and "short duct," are shown in figures 5 and 6.

Three interchangeable body flats ahead of the inlet were investigated. These approaches, lettered A, B, and C, provided two heights of the boundary-layer scoop and varied slightly the direction of flow approaching the inlet (see following table and fig. 3):

Approach surface	Angle between flat and body centerline, deg	Splitter height ¹		Splitter tested
		in.	h/ δ	
	2.22	0.68	1.2	Long and short
	1.28	.39	.68	Short
	0	.68	1.2	Short

¹ δ taken at M_0 of 1.99 and α of 0° .

In this report, the "basic configuration" is defined as that using approach A, the short splitter plate, and the open-sided boundary-layer diverter.

Internal Boundary-Layer Removal

Air was bled at the diffuser throat in attempts to improve pressure recovery. Flush slots or a ram scoop on the ceiling at the throat dumped the bled air into the boundary-layer channel on both sides of the diverter (figs. 7(a) and (b)). The area of the flush slots was about 17 percent of the throat area. The ram scoop was tested with a lip height of 0.3 and 0.5 inch, which gave capture areas of 10 and 17 percent of the inlet throat area, respectively. A flush slot on the compression surface (fig. 7(a)) was also tested in conjunction with the flush ceiling openings.

With approach B, the height of the boundary-layer channel, as well as the splitter-plate height, was normally reduced (fig. 7(a)). An alternate fairing aft of the splitter (sketched in fig. 7(c)) opened the channel to the full height to give more area for the flow from the ceiling slots.

In one phase of the test program, air was removed at the diffuser exit as might be done for a secondary-air supply or as a bypass for inlet-engine matching. For this purpose an annular manifold with flush bleed slots was installed just ahead of the diffuser-exit rake assembly (fig. 8). The bypassed air was discharged axially into the base region of the model.

External and Internal Flow Surveys

The airflow ahead of the inlet with approach A was surveyed by means of the rake and wedge shown in figure 9(a). The diffuser-exit rakes (fig. 9(b)) supported the centerbody representing the accessory housing. Except for two tubes nearest the centerbody, the tubes in the exit rakes were located at centroids of equal areas. Flow at the inlet throat was surveyed for the basic configuration with the rakes shown in figure 9(c). One of the side rakes was a dummy, installed to ensure flow symmetry. Pressure transducers were located near the throat and exit of the diffuser to sense unstable flow. These dynamic pressures were recorded with an oscillograph and a pen-type recorder. Unstable subcritical flow indicated by these instruments was generally verified by observing the shock structures in the schlieren system.

Test Conditions and Data Reduction

Data were obtained in the test program at Mach numbers of 1.99, 1.79, and 1.50 at angles of attack between -3° and 10° . The Reynolds number was about 5 million per foot. Total-pressure recoveries were computed from an area-weighted average of the tubes at the exit rake. Mass flows are based on this total-pressure recovery and the choked area at the exit plug. Duct mass flows are referenced to the free-stream flow that would pass through an area equal to the projection of the inlet area on a plane normal to approach A. In the computation of model drag from the balance forces, the base force was excluded, as was the change in momentum of the internal flow from the free stream to the diffuser exit.

RESULTS AND DISCUSSION

Flow Survey Ahead of Inlet

Results of the fuselage flow survey with approach A are given in figure 10. Mach numbers and flow angles determined by the wedge are shown in figure 10(a); rake profiles and resultant boundary-layer thickness are presented in figures 10(b) and (c), respectively. Fuselage Mach numbers were greater than free-stream values at angles of attack up to about 7° ; a maximum increase of about 0.035 was noted. Despite the inward turning (2.22°) of approach A, the flow at the survey-wedge position was nearly aligned in the free-stream direction at zero angle of attack. At 10° body angle of attack the flow angle at the survey wedge was at 5° to the fuselage centerline. The measured Mach numbers and Pitot profiles indicate only a slight loss in total pressure ahead of the inlet - less than 1 percent at Mach number 1.99 at $\alpha = 0^\circ$. Although the boundary layer was measured only with approach A, the thickness shown in figure 10(c) can be expected to be approximately true for approaches B and C. Resultant values of h/δ at Mach number 2.0 are about 1.2 for approaches A and C and 0.68 for approach B.

Alternative Configurations

Total-pressure recoveries and drags obtained with approach A (short and long splitter) and with approaches B and C (short splitter) are shown in figures 11 to 14. In these and subsequent figures, flow instabilities $\Delta p_2/P_0$ greater than 5 percent are shown by solid symbols. Schlieren photographs of the basic configuration are shown in figure 15. Peak and critical pressure recoveries at zero angle of attack are summarized in figure 16.

3971

Pressure recovery. - Peak recoveries under stable conditions were essentially the same with the two splitters of approach A (fig. 16). Comparable or slightly better recoveries were obtained with approach B, even though at zero angle of attack some fuselage boundary layer was ingested. With approaches A and B, peak pressure recoveries decreased from 0.93 to about 0.78 (at α of 0°) with the increase in Mach numbers from 1.50 to 1.99. These recoveries are, respectively, 98 and 90 percent of the theoretical maximum for inviscid flow available from a 14.2° -wedge inlet at the fuselage flow conditions. Generally higher recoveries over the Mach number and angle-of-attack ranges were obtained with approach C. For example, at M_0 of 1.99 and α of 0° , the peak pressure recovery was increased to 0.805. Although the fuselage flow was not surveyed with approach C, these improvements are probably due to a lower fuselage Mach number with approach C (less expansion ahead of the inlet) and a concomitant increase in the effective compression angle of the inlet toward the angle for best recovery.

Stability. - Flow instability could result from interaction of the terminal shock with the boundary layer of either the splitter plate or the fuselage. For example, consider the results of reducing the mass-flow ratio of the basic configuration at Mach 1.99 and zero angle of attack (see fig. 15): From critical flow (0.967) down to the mass flow at which the normal shock moved ahead of the splitter (0.903), unstable boundary-layer separation was observed. Resulting measured flow instabilities $\Delta p_2/P_0$ were generally less than 0.05. Stable interaction of the normal shock with the fuselage boundary layer then occurred until the mass-flow ratio was reduced below about 0.825. At that point violent shock pulsing ensued; values of $\Delta p_2/P_0$ as high as 0.2 or more were measured. The sharp rise in subcritical pressure recovery shown at Mach number 1.99 for all configurations is the measured average under such unstable conditions and, hence, probably does not represent useful operating pressure recoveries for the inlet.

For purposes of comparison, a stable mass-flow ratio can arbitrarily be taken to be one for which the value of $\Delta p_2/P_0$ is less than 0.05, although, as discussed, unstable separation of the splitter-plate boundary layer may be occurring. With this definition, both the basic configuration and that with approach B gave a stable range of about 0.13 m_0 at Mach 1.99 and zero angle of attack. This range was almost doubled by use of the long splitter or approach C. Appreciable improvements were also obtained at Mach number 1.79 by the use of these latter two configurations. The inlet was free of buzz at Mach 1.50, although the normal shock (which could not be swallowed at this Mach number) separated the fuselage boundary layer with all configurations (e.g., fig. 15(c)).

Drag. - Approach B appeared to give slightly lower drags than the other configurations. This could be attributed to the fact that less air was handled by the boundary-layer-removal system. Appreciable scatter in the drag data is shown in some instances. The accuracy of the drag data was adversely affected by the flow instabilities discussed and uncertainties in the exit momentum of the internal flow that resulted from the wide variation (supercritically) in static pressure at the diffuser exit (e.g., pressure contour, fig. 19(a)).

Miscellaneous data. - Pressure recoveries of those configurations investigated at the subsonic Mach number of 0.63 are shown in figure 17. No appreciable differences were noted except for a slight improvement obtained with the long splitter. The experimental recoveries were slightly higher than those predicted by the theory of reference 7 for sharp-lip inlets.

No significant effect on drag or pressure recovery was found when the boundary-layer channel of the basic configuration was enclosed to form the "long" duct or "short" duct (see figs. 5 and 6). The Mach 1.99 data of figure 18 are typical.

Internal-Flow Details of Basic Configuration

The effects of mass-flow ratio on the total-pressure distributions at the inlet and at the compressor-face station are shown in figure 19 for the basic configuration at zero angle of attack and Mach 1.99; corresponding schlierens are also presented. The effects of Mach number and angle of attack on the exit contours at critical flow are shown in figure 20.

With decreasing mass flow (figs. 19(a) to (c)), there is a progressive decrease in the total-pressure distortion $\Delta P/P_2$ at the diffuser exit; a value of 17 percent was observed at peak pressure recovery. (Similar distortion values were noted with the other configurations.) With decreasing mass flow there is also a shift of high energy from the top to the bottom of the exit, which occurs at all Mach numbers and angles of attack. The asymmetrical subcritical flow is shown in figure 19(c) to result from the sharp demarcation at the throat between the normal-shock recovery and the recovery behind the oblique- and normal-shock system. The adjacent exit contour plot shows that very little mixing of these flow fields occurs in the subsonic diffusion process. At critical mass flows (fig. 20), total-pressure contours are generally symmetrical about the horizontal centerline, with distortions ranging from about 11 to 18 percent over the Mach number and angle-of-attack range.

Air Bleed at Throat

Inasmuch as the inlet and exit profiles show that losses in total pressure can be attributed to interaction of the terminal shock with the boundary layer of the splitter plate, several throat-bleed "fixes" were tried in an attempt to minimize these losses. Flush bleed slots and ram scoops were installed on the ceiling at the inlet throat (fig. 7). The terminal-shock - boundary-layer interaction on the compression surface also could be expected to adversely affect pressure recovery, as happens with conventional ramp- or spike-type inlets. For these latter types, references such as 8 and 9 show appreciable gains in total-pressure recovery and in thrust-minus-drag with the bleeding of air from the compression surface at the throat. Accordingly, a flush bleed slot on the compression surface was also investigated with this model. Results obtained with the throat-bleed configurations (flush slots with approaches A and B, ram scoops with approach A only) are given in figures 21 and 22. Drag data were not available in all cases; the complete Mach number and angle-of-attack ranges were not investigated for all configurations.

The effectiveness of the flush ceiling slot in improving pressure recoveries increased with free-stream Mach number. Greater gains were realized with approach B (fig. 22(a)) than with approach A (fig. 21(a)), although the former configuration bypassed only about half as much air ($0.02 m_0$) at critical flow. At Mach 1.99, pressure recoveries of 0.81 and 0.84 were obtained at $\alpha = 0^\circ$ for approaches A and B, respectively. Increasing the height of the boundary-layer channel with approach B (fig. 22(b)) did not significantly affect pressure recoveries.

As with the no-bleed configurations, unstable separation of the splitter-plate boundary layer occurred with the flush ceiling slot; at Mach 1.99, this separation induced pressure fluctuations exceeding $0.05 P_0$ for some mass flows between critical and that for peak pressure recovery. At M_0 of 1.99, peak recovery occurred with the terminal shock slightly ahead of the splitter plate.

The flush slot in the compression surface was tested only in conjunction with the flush ceiling slot and approach A. Despite the bypass of considerable flow ($0.13 m_0$ at critical), there was no improvement in the pressure recovery over that of the basic configuration (fig. 21(b)). In addition, there was no subcritical stability. Limitations imposed by model construction prevented a detailed study of bleed on the compression surface; but, based on the results obtained with other inlet types, there is good reason to believe that pressure recoveries could be improved with this technique.

Both ram scoops increased the pressure recovery to about 0.83 at Mach 1.99 at zero angle of attack (fig. 21(c) and (d)). Supercritical

bypass of air was about 4 and 7 percent of the captured mass flow for the scoop heights of 0.3 and 0.5 inch, respectively. The stable subcritical range was about the same as with the basic configuration.

Air Bypass at Engine Face

Figure 23 shows the pressure recoveries obtained with the bypassing of air at the diffuser exit with the basic configuration. About 8 percent of the critical flow was bypassed at all Mach numbers. A slight improvement in total-pressure recovery is shown at Mach numbers 1.50 and 1.79, but none at Mach 1.99. A study of the total-pressure profiles at the diffuser exit showed very little effect of this amount of bleed on the profiles or the distortions. These results agree generally with data of such references as 10 to 12, which indicate that bypassing air near the diffuser exit of a variety of configurations is an effective scheme for engine-inlet matching but provides little if any improvement in total-pressure recoveries.

SUMMARY OF RESULTS

A scoop inlet having a semielliptic projected frontal shape was investigated on the bottom of a missile fuselage model at Mach numbers of 0.63 and 1.50 to 1.99 at angles of attack to 10° . Included in the investigation was a study of the effects of altering the approach surface ahead of the inlet, varying the length and height of the boundary-layer splitter plate, and bleeding air at the throat and exit of the diffuser. Results of the test program may be summarized as follows:

1. With the configuration having a 2.22° inward turning of the body flat and full removal of the fuselage boundary layer, peak total-pressure recoveries of 0.93, 0.875, and 0.78 were obtained at Mach numbers of 1.50, 1.79, and 1.99 at zero angle of attack. Peak pressure recoveries were generally insensitive to angle of attack for the no-bleed configurations.

2. Pressure recovery increased slightly and the stable range doubled as inward turning of the body flat was changed from 2.22° to 0° at Mach 1.99 and at zero angle of attack.

3. Subcritical flow instabilities, primarily found at Mach 1.99, were caused by terminal-shock-induced separation of the boundary layer of either the splitter plate or the fuselage. Pressure fluctuations with the fuselage separation were so severe as probably to preclude operation under these conditions. The most stable configuration was thus limited to a useful subcritical range of about 20 percent of its critical flow at Mach 1.99.

4. Increasing the boundary-layer splitter-plate length (about 1.3 fuselage boundary-layer thicknesses) increased the subcritical stable range without affecting maximum pressure recoveries. Essentially the same pressure recoveries were obtained with splitter-plate heights of either 1.2 or 0.68 boundary-layer thickness (thickness measured at Mach 1.99 and zero angle of attack).

5. Bleeding air from either flush slots or ram scoops at the inlet throat increased the peak pressure recovery at Mach 1.99 from 0.78 to about 0.83. The stable mass-flow range was considerably reduced with the flush slots but was essentially the same with the ram scoop.

Lewis Flight Propulsion Laboratory
National Advisory Committee for Aeronautics
Cleveland, Ohio, December 14, 1956

REFERENCES

1. Anon.: Survey of Bumblebee Activities. Bumblebee Rep. No. 89, Appl. Phys. Lab., The Johns Hopkins Univ., Oct. 1948. (Contract NORD 7386 with Bur. Ord., U.S. Navy.)
2. Dailey, C. L., Douglass, Wm. M., and McFarland, H. W.: Preliminary Investigation of Scoop Type Supersonic Diffusers. USCAL Rep. 11-1, Aero Lab., Univ. Southern Calif., Dec. 15, 1951. (Summary Rep. USN BuAer Contract NOa(s) 12044.)
3. Comenzo, Raymond J., and Mackley, Ernest A.: Preliminary Investigation of a Rectangular Supersonic Scoop Inlet with Swept Sides Designed for Low Drag at a Mach Number of 2.7. NACA RM L52J02, 1952.
4. Kochendorfer, Fred D.: Investigation at a Mach Number of 1.90 of a Diverter-Type Boundary-Layer Removal System for a Scoop Inlet. NACA RM E53D07, 1953.
5. Curtiss-Wright Corp.: Some Recent Advances in the Design of Supersonic Diffusers. Wright Aero. Rep. No. 1692, Supersonic Inlet Symposium, Wood-Ridge (N. J.), Jan. 23, 1953.
6. Curtiss-Wright Corp.: Design and Analysis of Three Supersonic Side Inlet Diffuser Models. Wright Aero. Rep. No. 1755, Sept. 22, 1953.
7. Fradenburgh, Evan A., and Wyatt, DeMarquis D.: Theoretical Performance Characteristics of Sharp-Lip Inlets at Subsonic Speeds. NACA Rep. 1193, 1954. (Supersedes NACA TN 3004.)

8. Obery, Leonard J., and Cubbison, Robert W.: Effectiveness of Boundary-Layer Removal Near Throat of Ramp-Type Side Inlet at Free-Stream Mach Number of 2.0. NACA RM E54IL4, 1954.
9. Campbell, Robert C.: Performance of Supersonic Ramp-Type Side Inlet with Combinations of Fuselage and Inlet Throat Boundary-Layer Removal. NACA RM E56A17, 1956.
10. Allen, J. L., and Beke, Andrew: Force and Pressure Recovery Characteristics at Supersonic Speeds of a Conical Spike Inlet with Bypasses Discharging in an Axial Direction. NACA RM E52K14, 1953.
11. Nettles, J. C., and Leissler, L. A.: Investigation of Adjustable Supersonic Inlet in Combination with J34 Engine up to Mach 2.0. NACA RM E54H11, 1954.
12. Allen, John L.: Performance of a Blunt-Lip Side Inlet with Ramp Bleed, Bypass, and a Long Constant-Area Duct Ahead of the Engine: Mach Numbers 0.66 and 1.5 to 2.1. NACA RM E56J01, 1956.

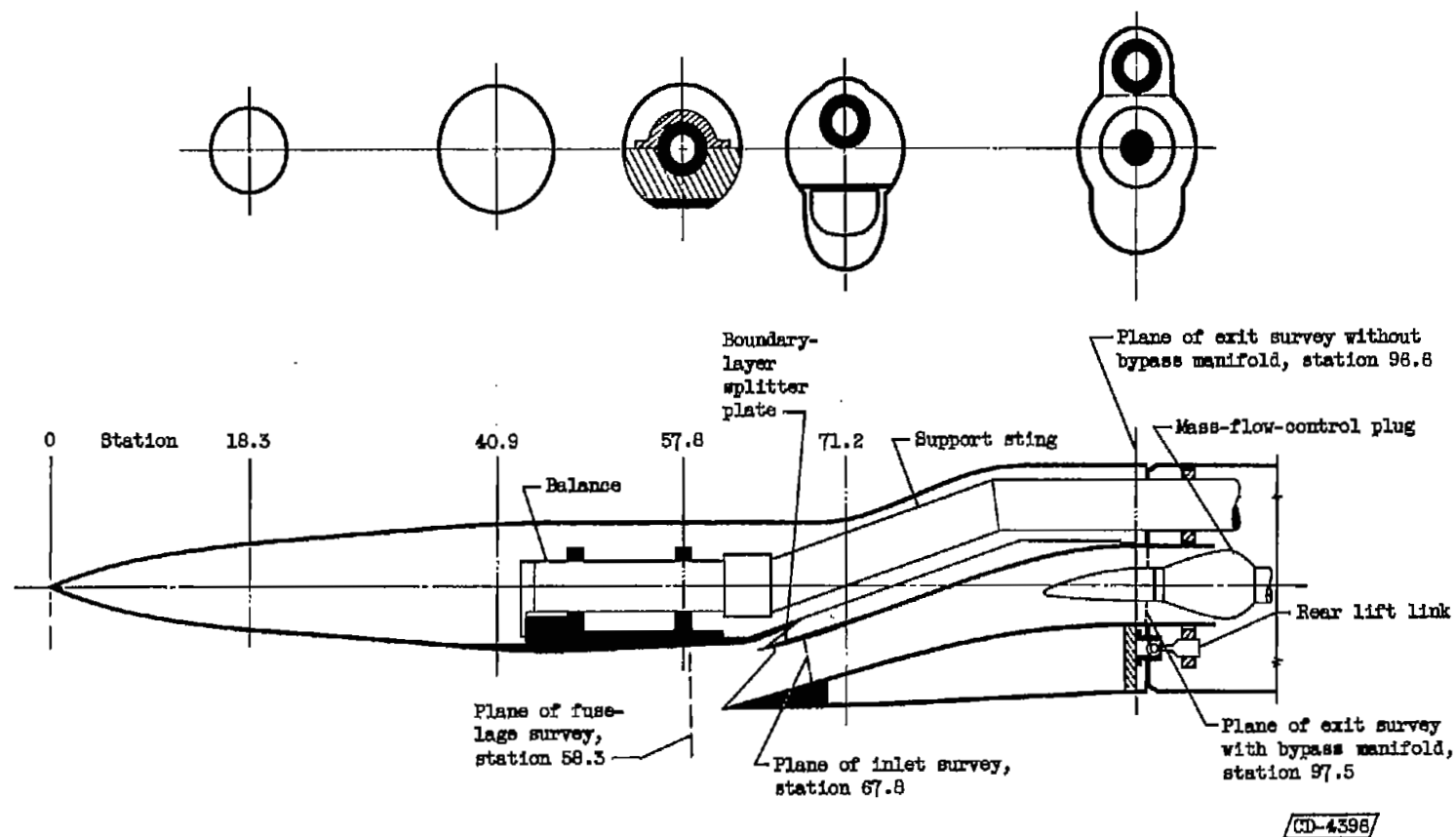


Figure 1. - Schematic drawing of model.



Figure 2. - Photographs of model.

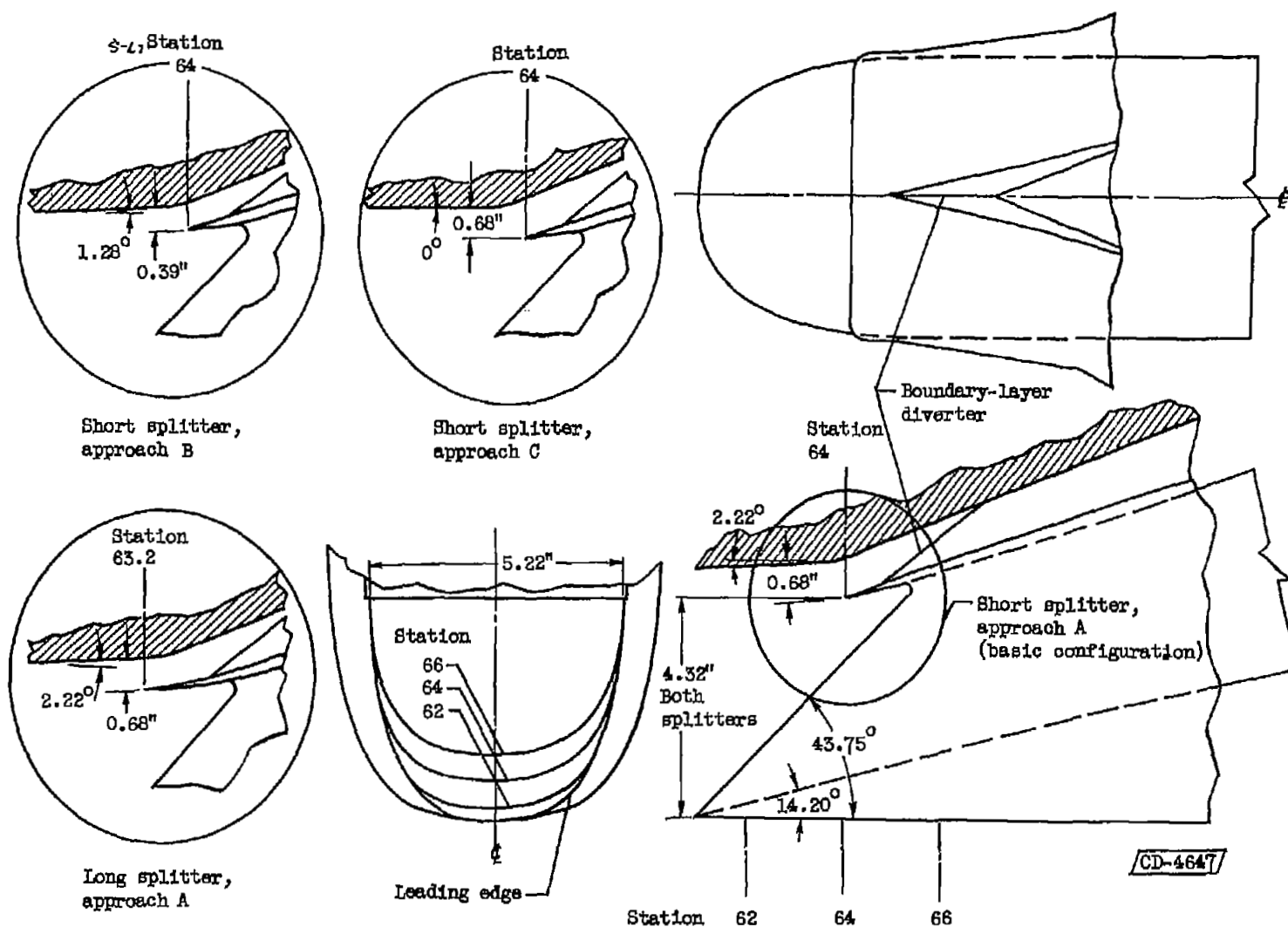


Figure 3. - Details of inlet.

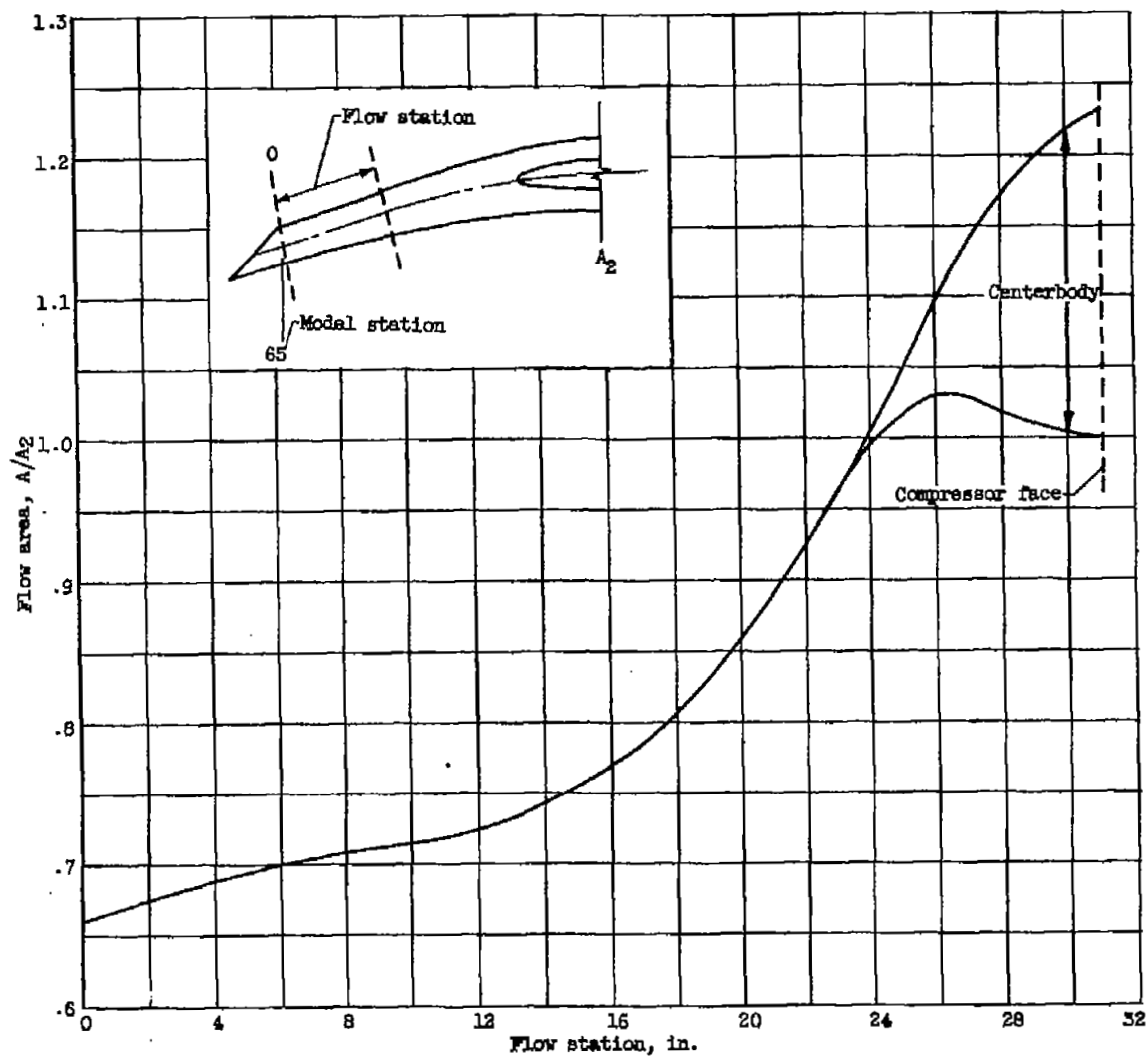


Figure 4. - Diffuser area variation.

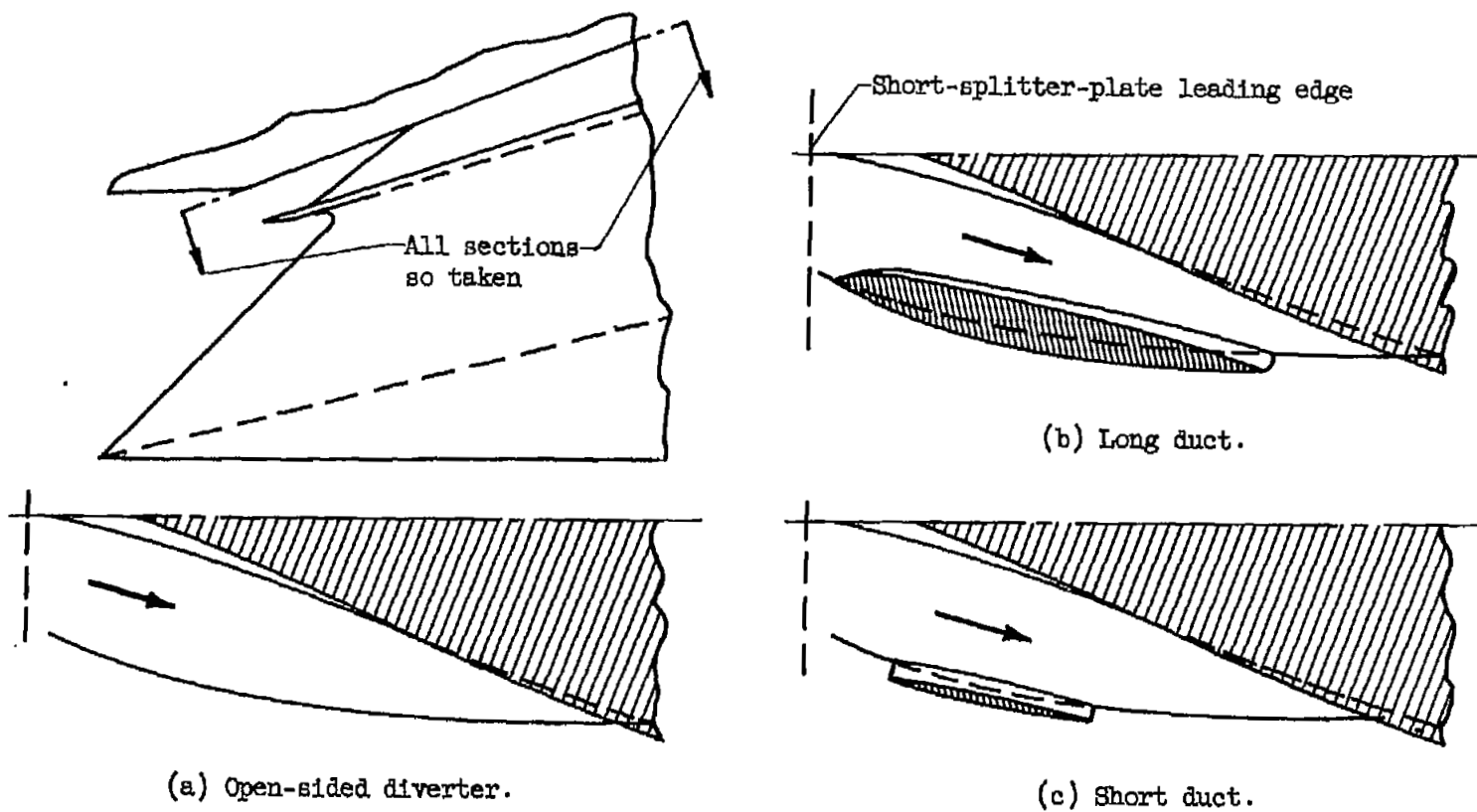
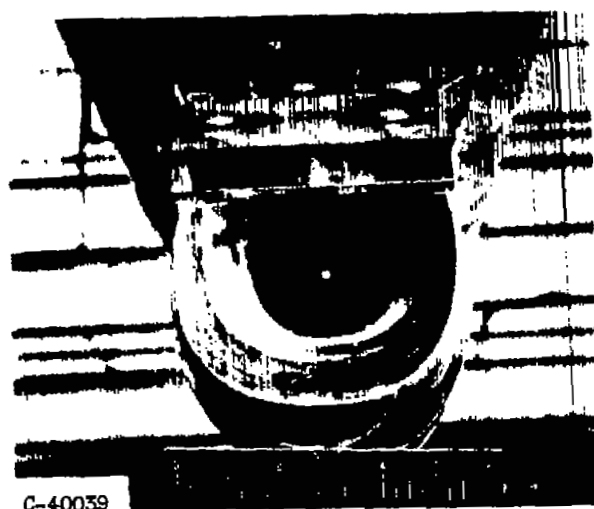


Figure 5. - Sketches of boundary-layer-removal systems.



C-40039



C-40037

(a) Long duct.



C-40038



C-40036

(b) Short duct.

Figure 6. - Boundary-layer duct systems.

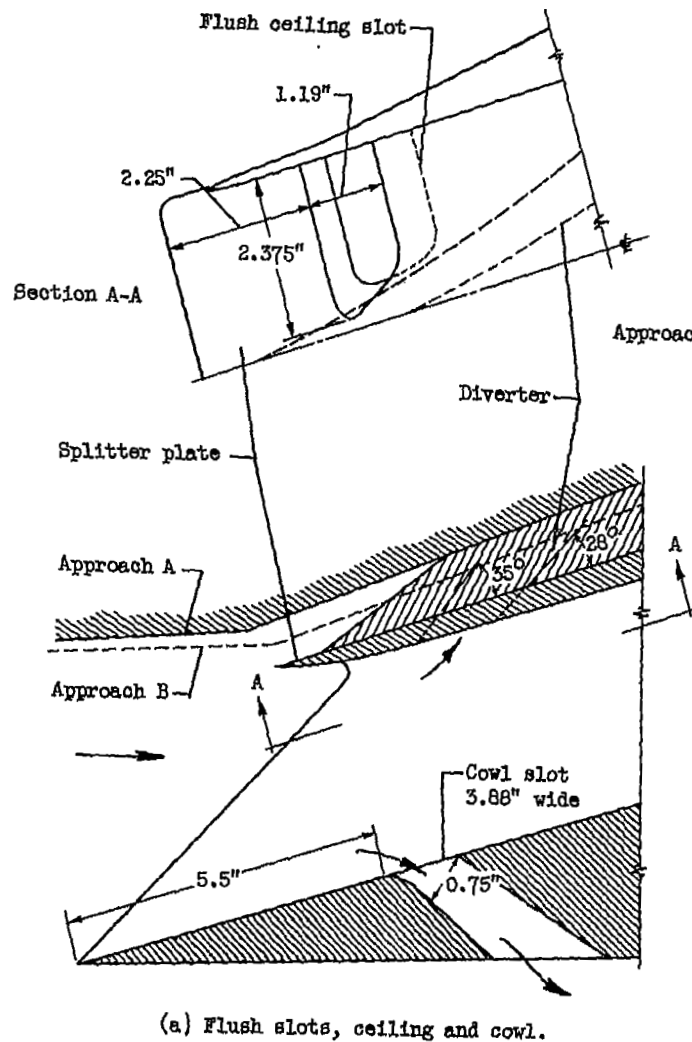
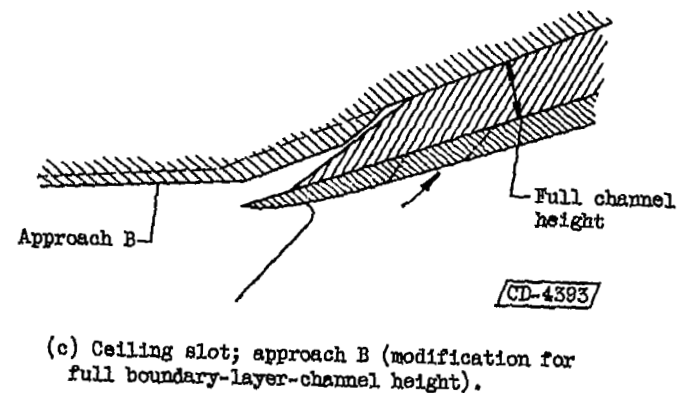
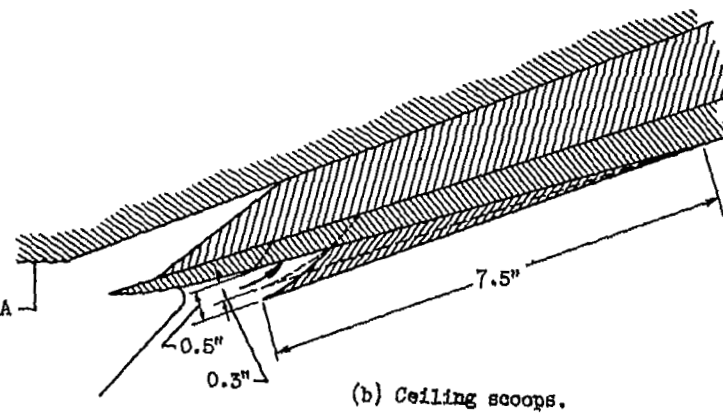


Figure 7. - Throat-bleed configurations.



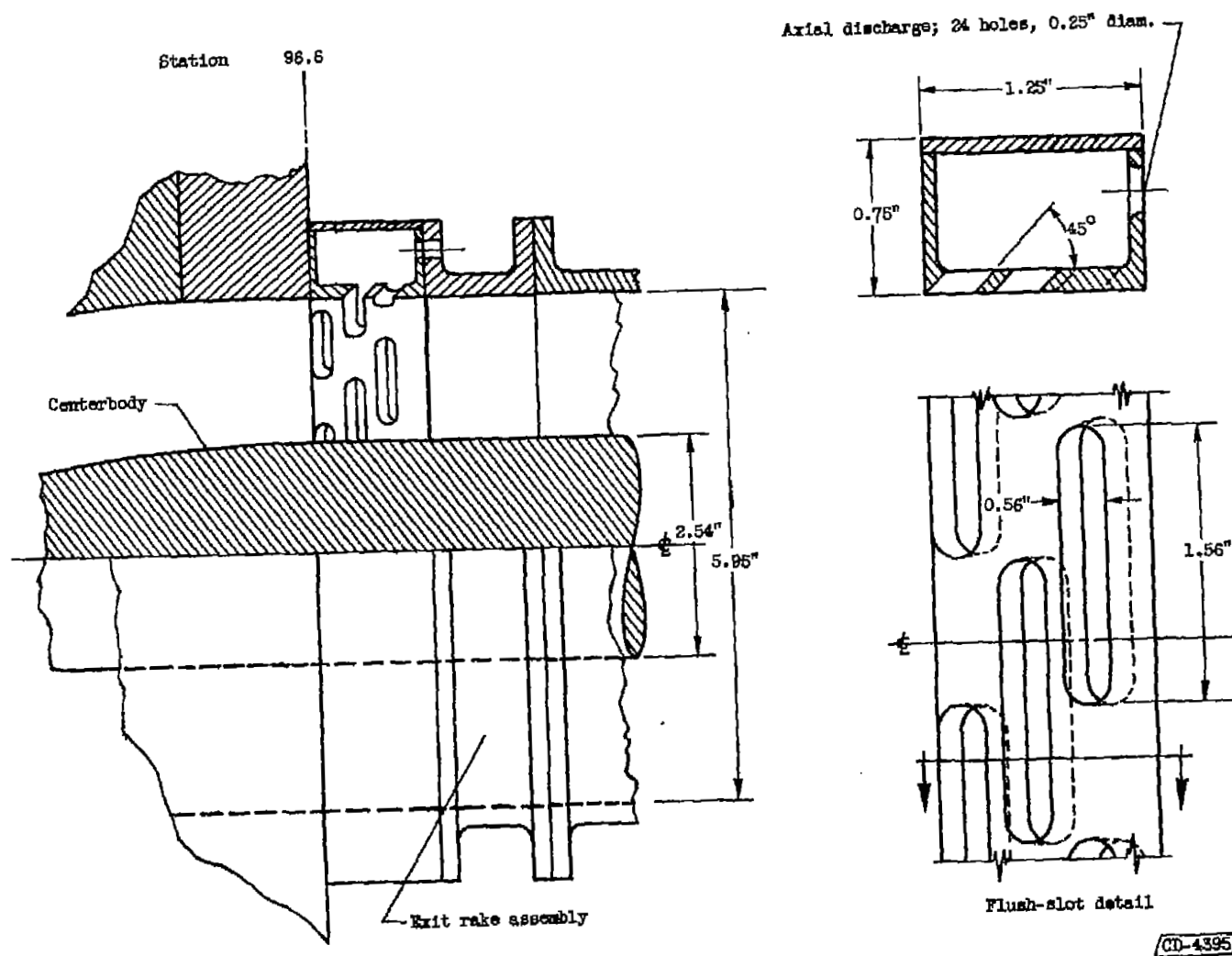
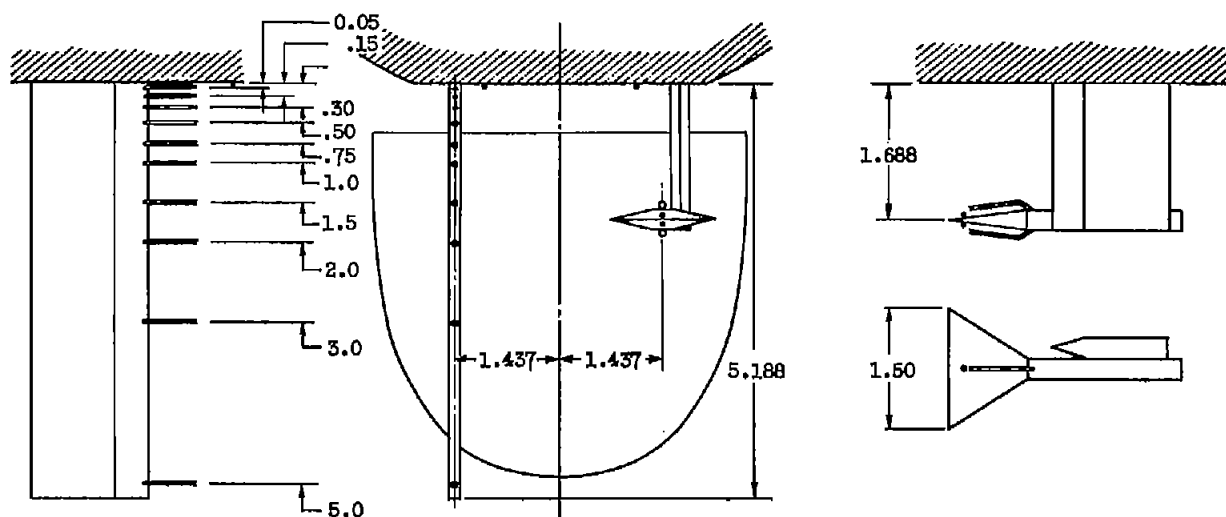
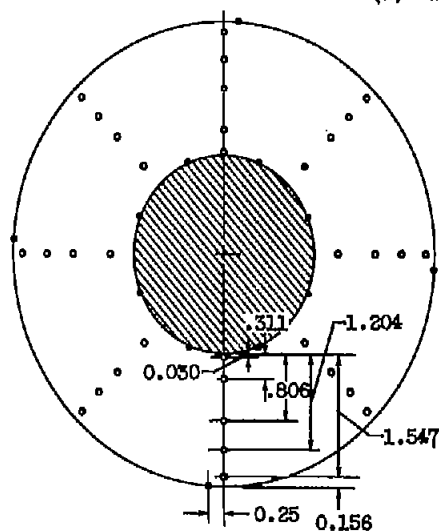


Figure 8. - Sketch of bypass manifold installation.

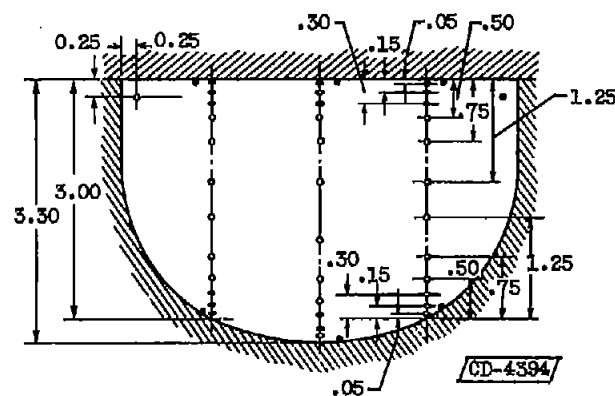


(a) Fuselage survey rake and wedge.

- Static orifice
- o-- Pitot tube

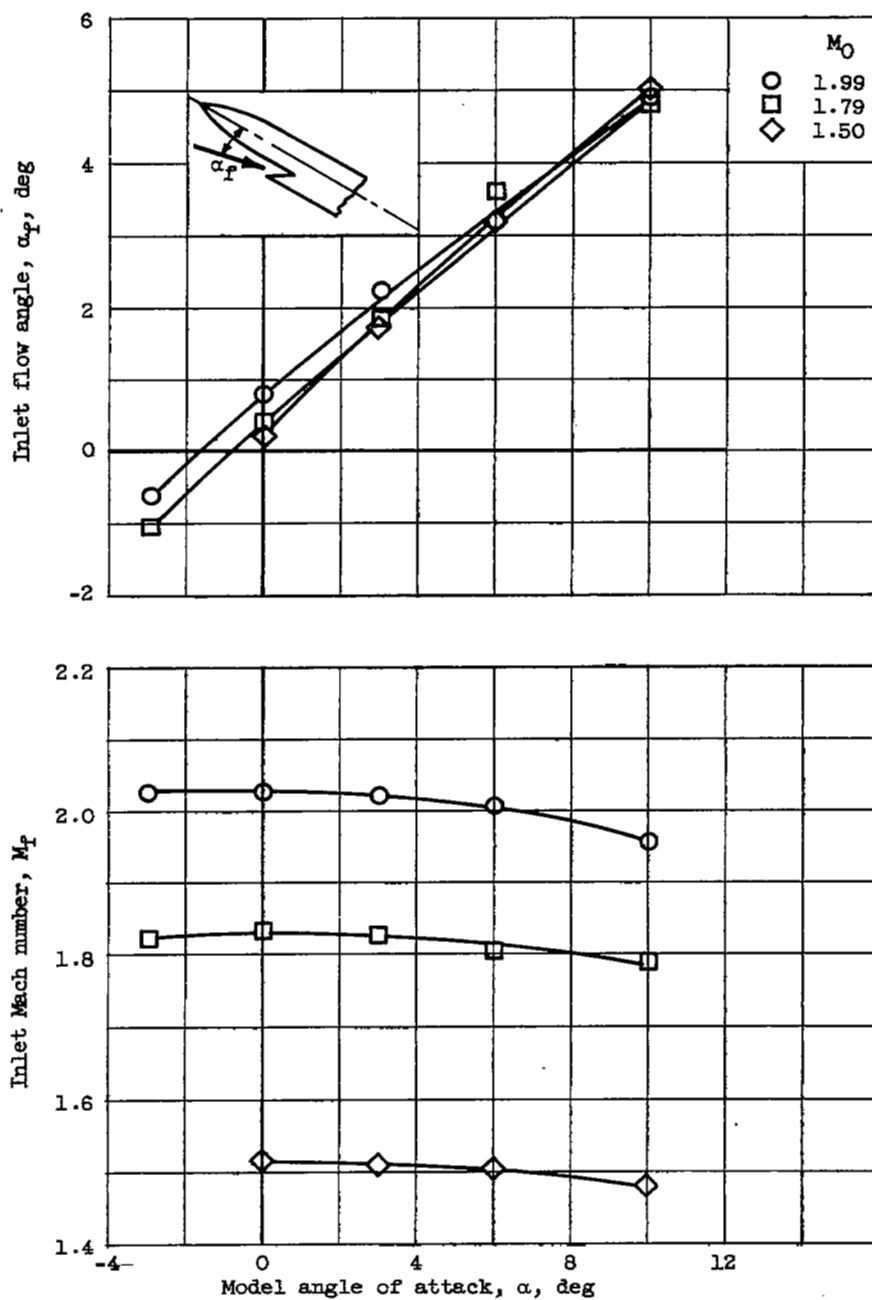


(b) Diffuser-exit rakes.



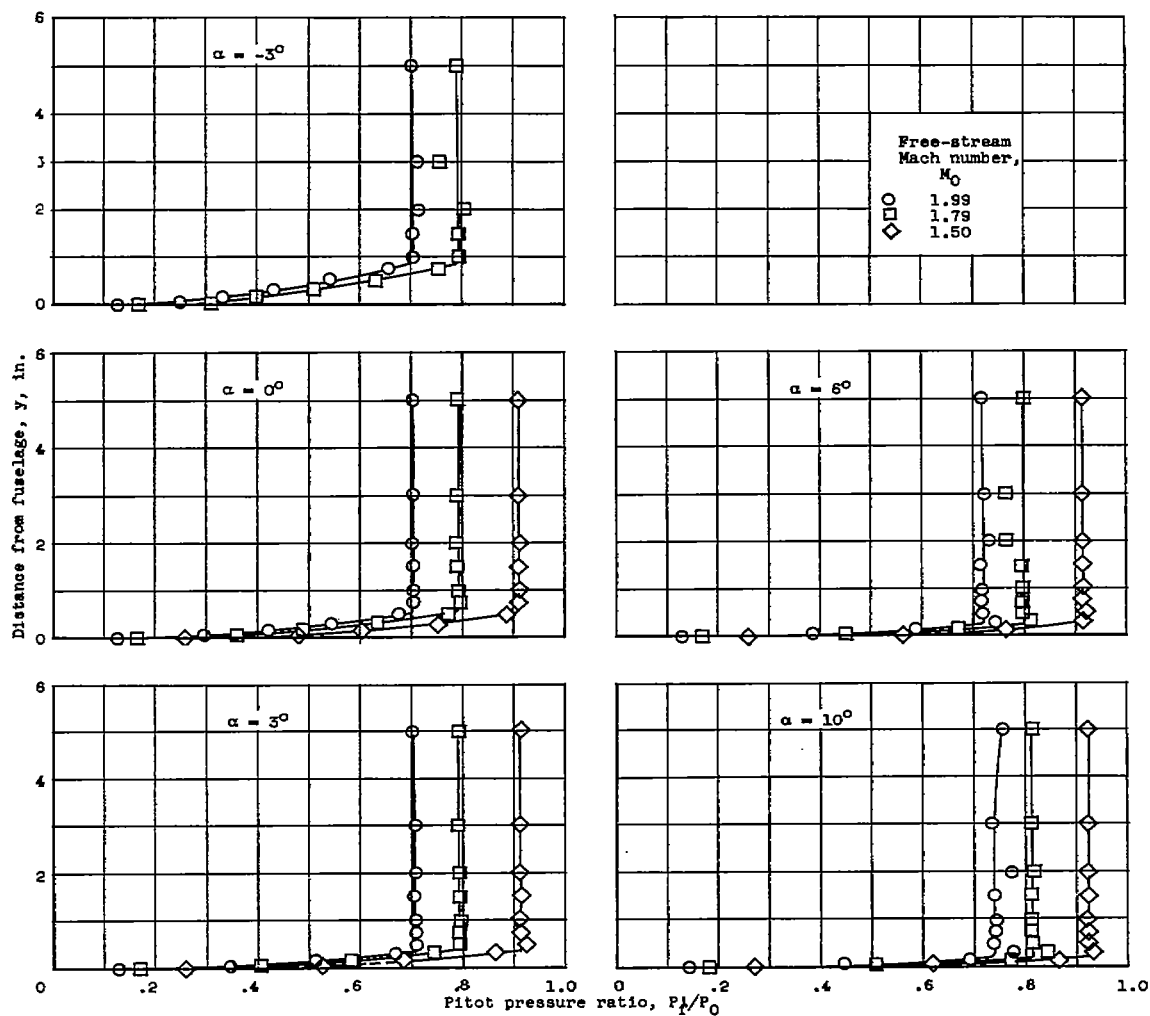
(c) Inlet rakes.

Figure 9. - Model instrumentation (all dimensions in inches).



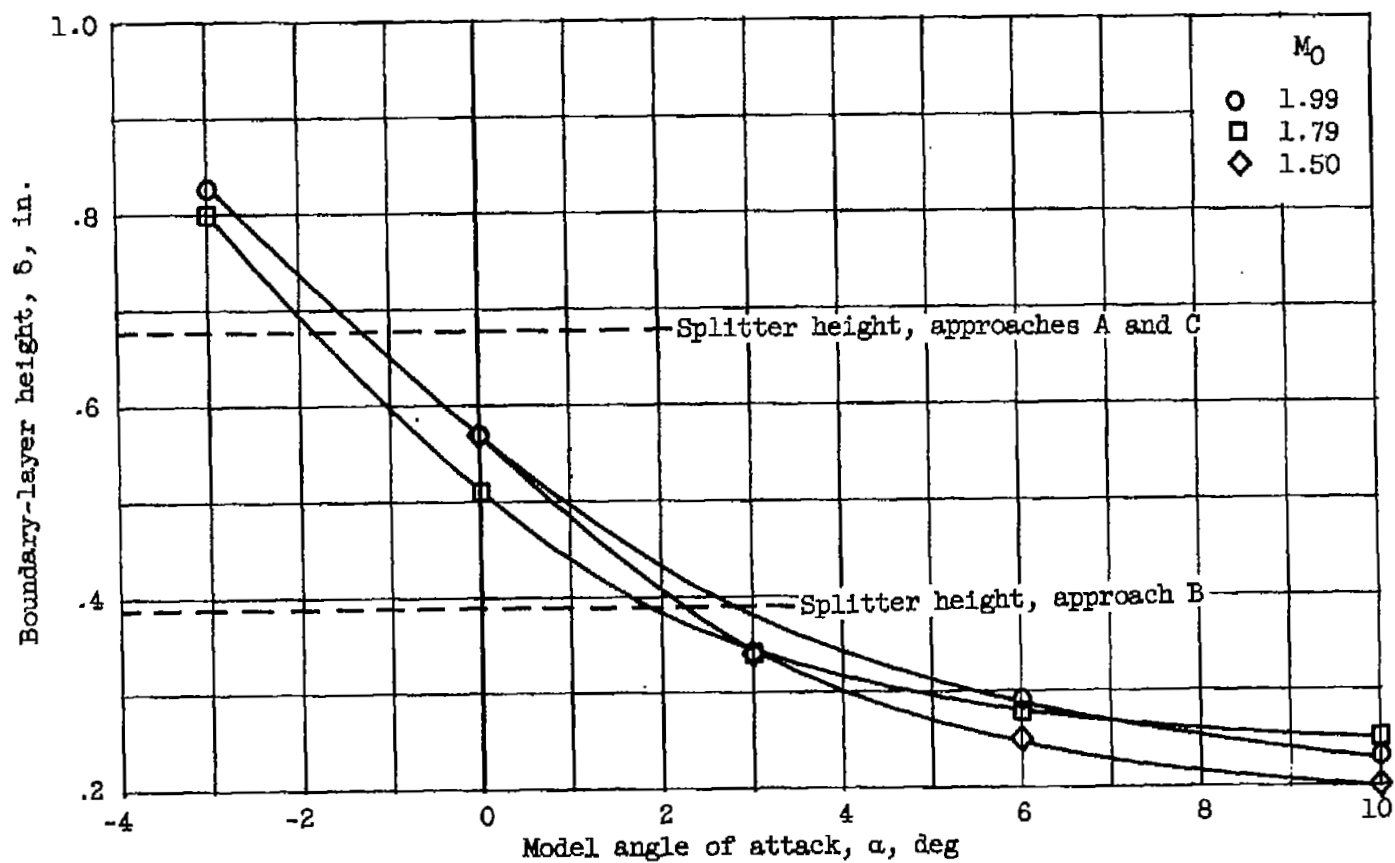
(a) Inlet Mach number and local angle of attack.

Figure 10. - Fuselage flow survey (with approach A).



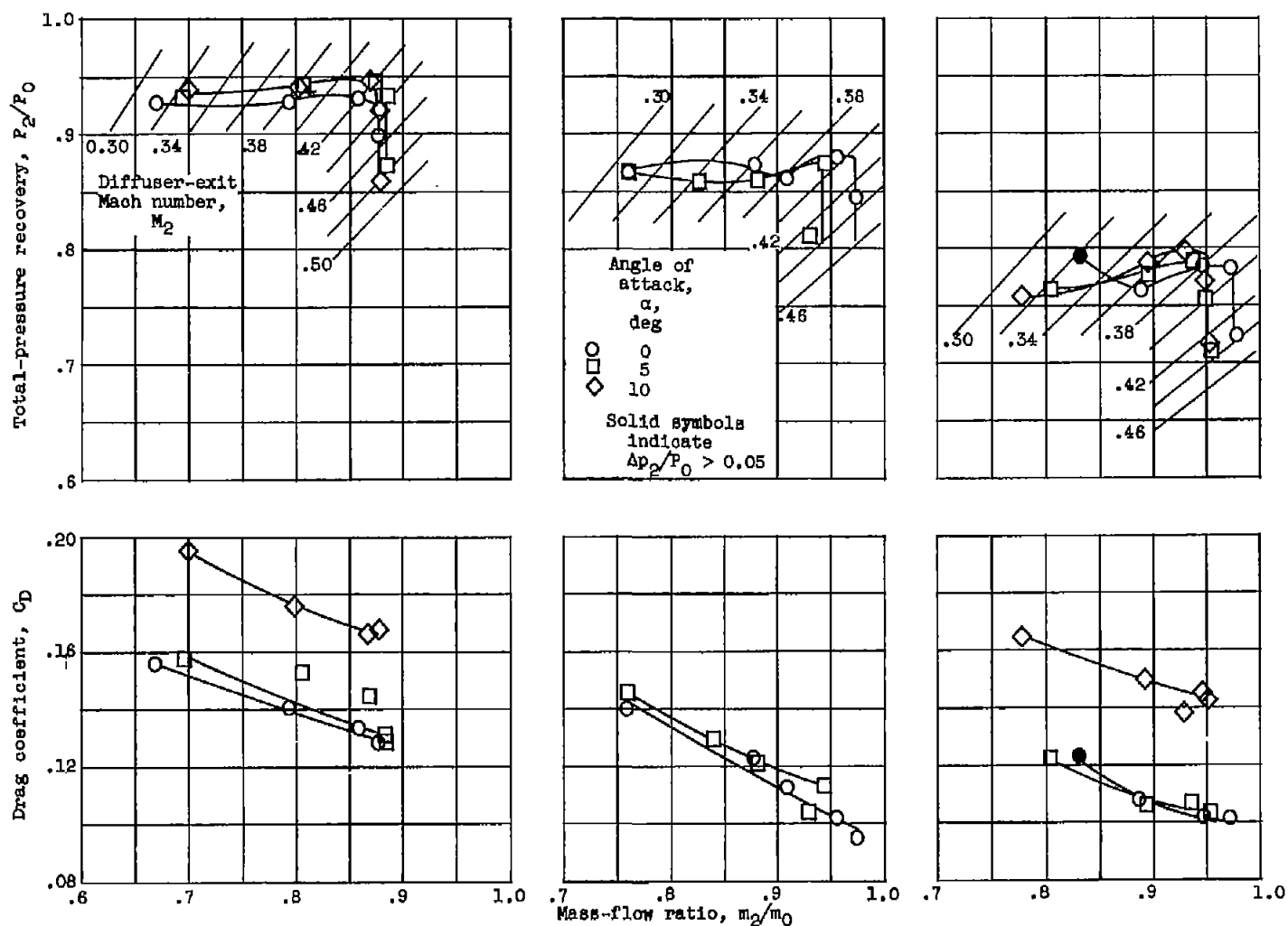
(b) Pitot pressure profiles.

Figure 10. - Continued. Fuselage flow survey (with approach A).



(c) Boundary-layer height.

Figure 10. - Concluded. Fuselage flow survey (with approach A).



(a) Free-stream Mach number, 1.50.

(b) Free-stream Mach number, 1.79.

(c) Free-stream Mach number, 1.99.

Figure 14. - Performance with short splitter and approach B.

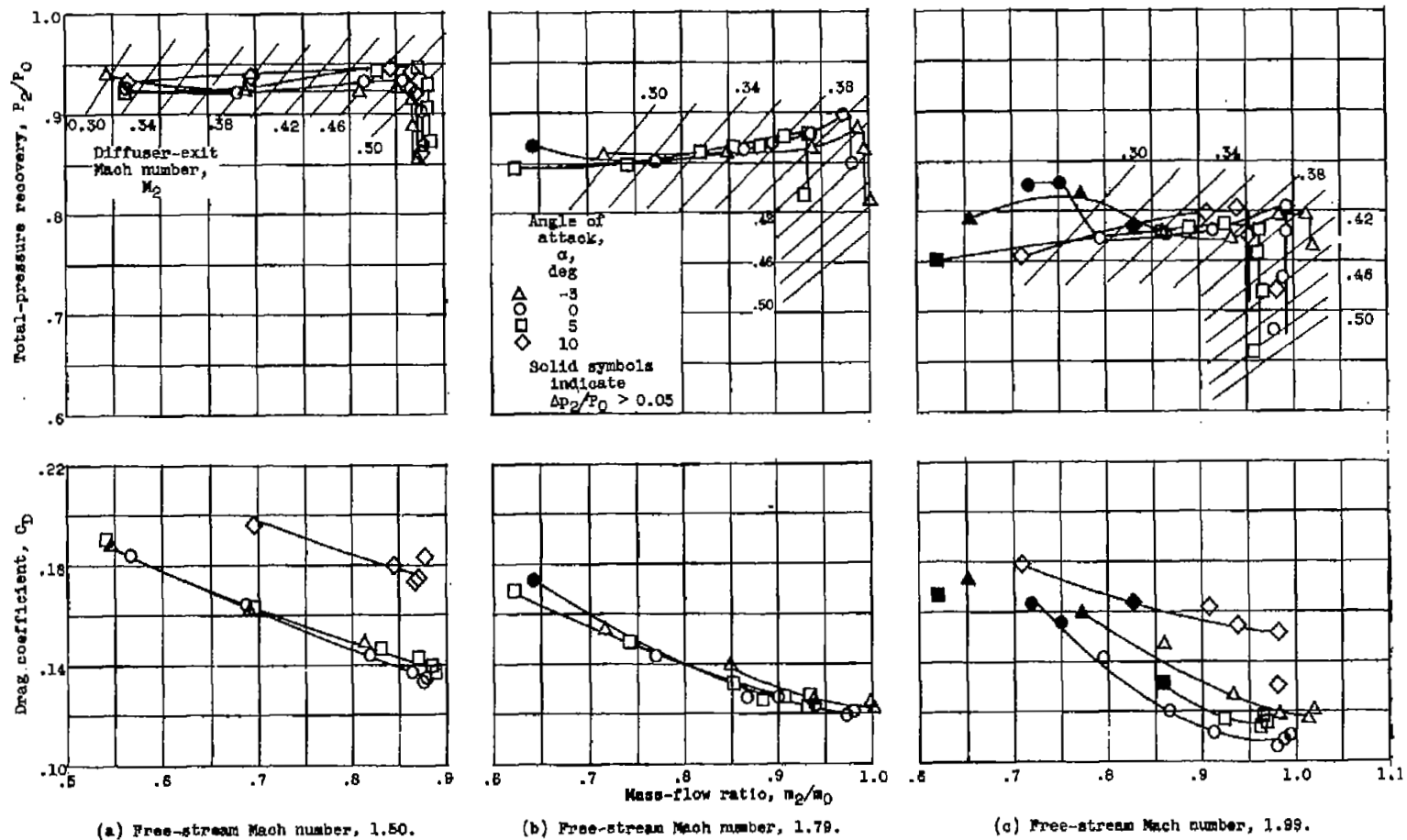


Figure 13. - Performance with short splitter and approach C.

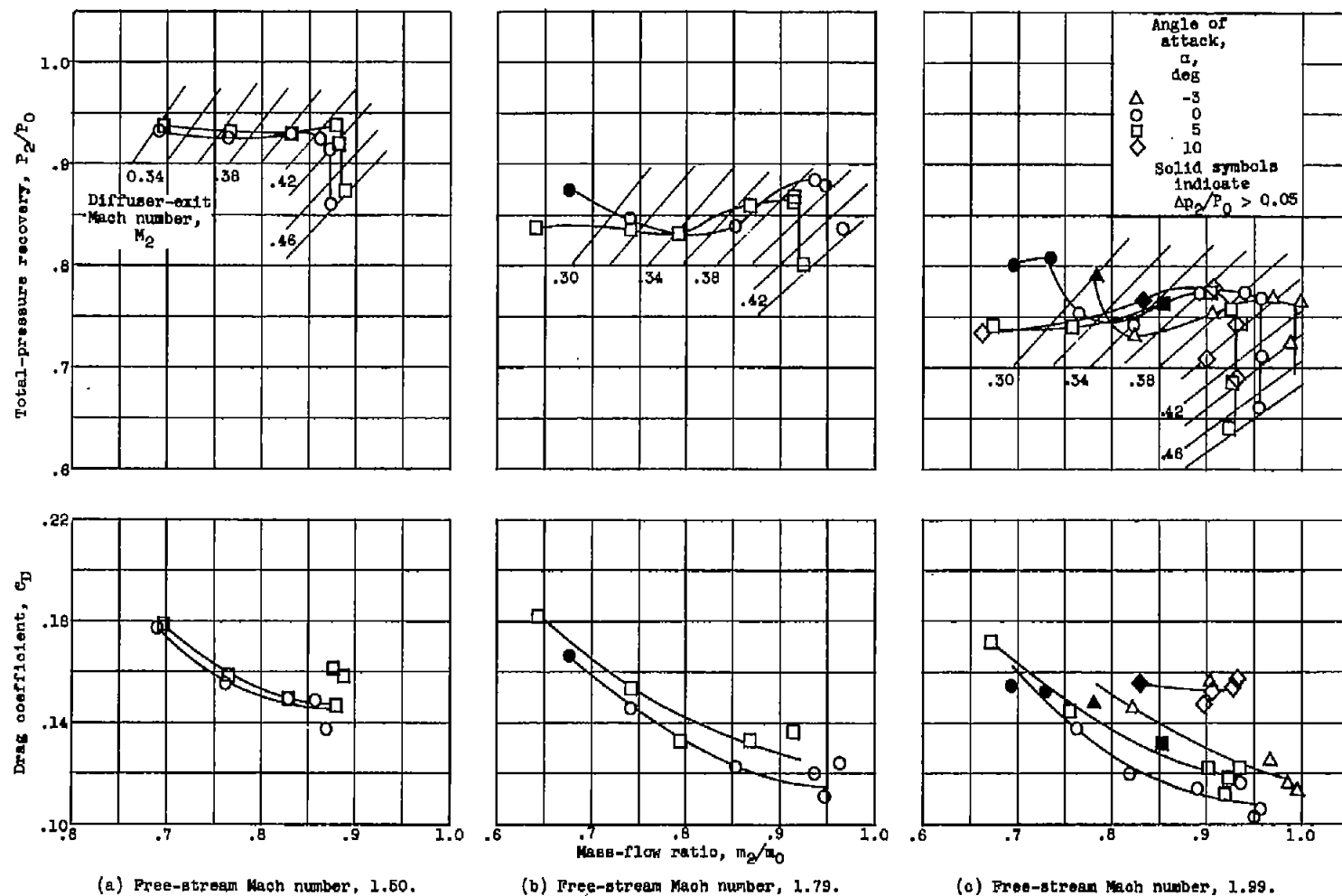


Figure 12. - Performance with long splitter and approach A.

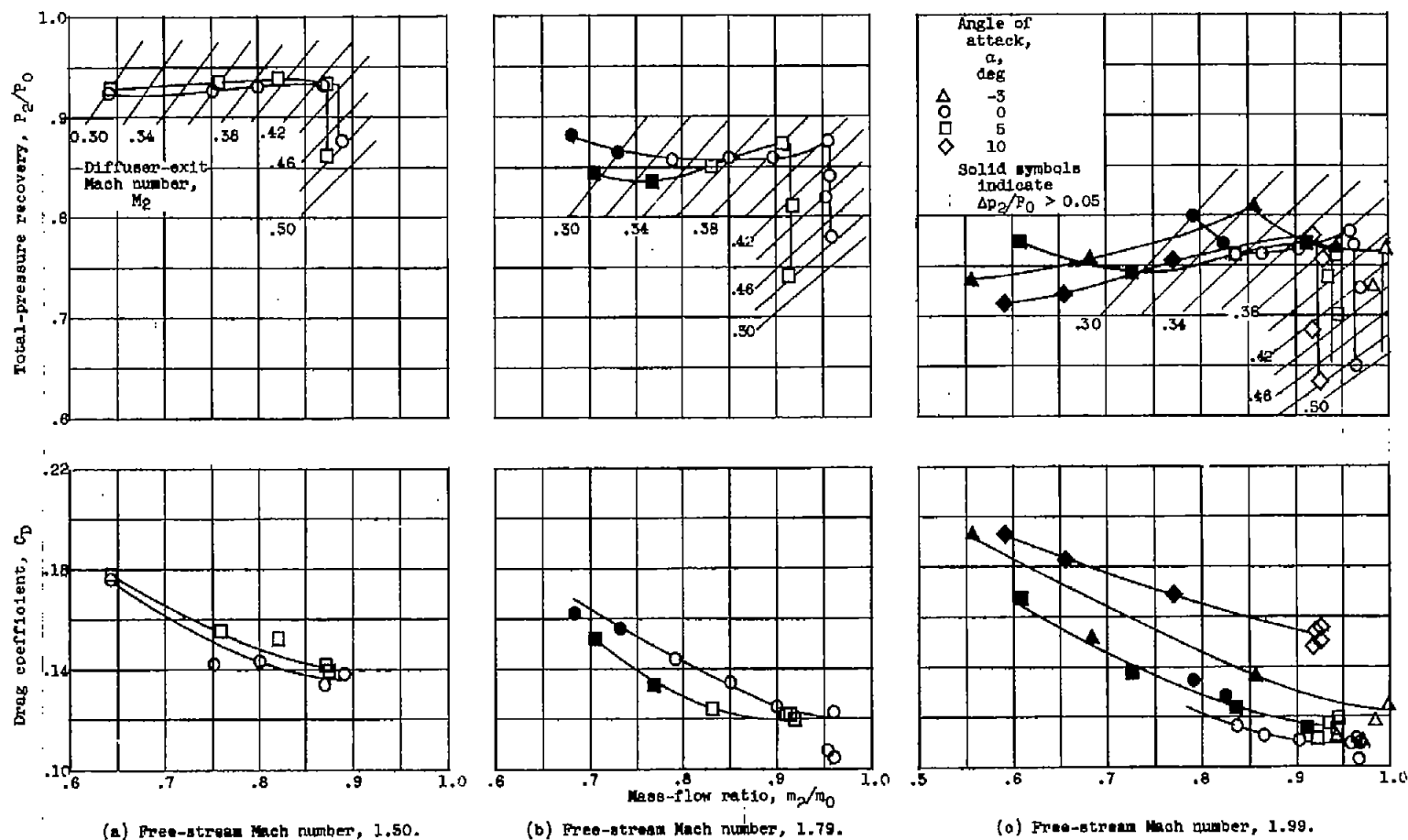


Figure 11. - Performance of basic configuration (short splitter and approach A).



Data point 1



2



3



4



5

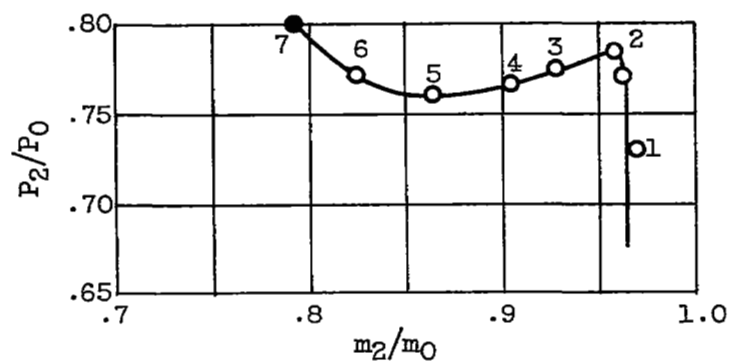


6



7

C-43516

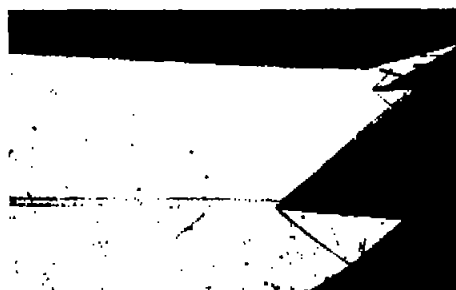


(a) Mass-flow range at free-stream Mach number of 1.99 and zero angle of attack.

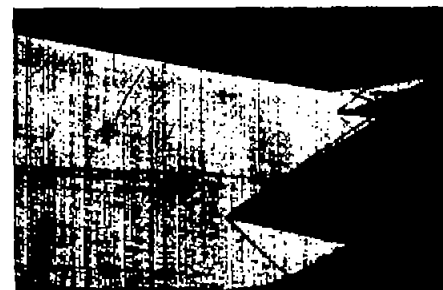
Figure 15. - Schlieren photographs of basic configuration.



$\alpha = -3^\circ$



$\alpha = 5^\circ$



$\alpha = 10^\circ$

(b) Supercritical flow at angle of attack; free-stream Mach number, 1.99.



$M_0 = 1.79$



$M_0 = 1.50$

(c) Supercritical flow at zero angle of attack.

Figure 15. - Concluded. Schlieren photographs of basic configuration.

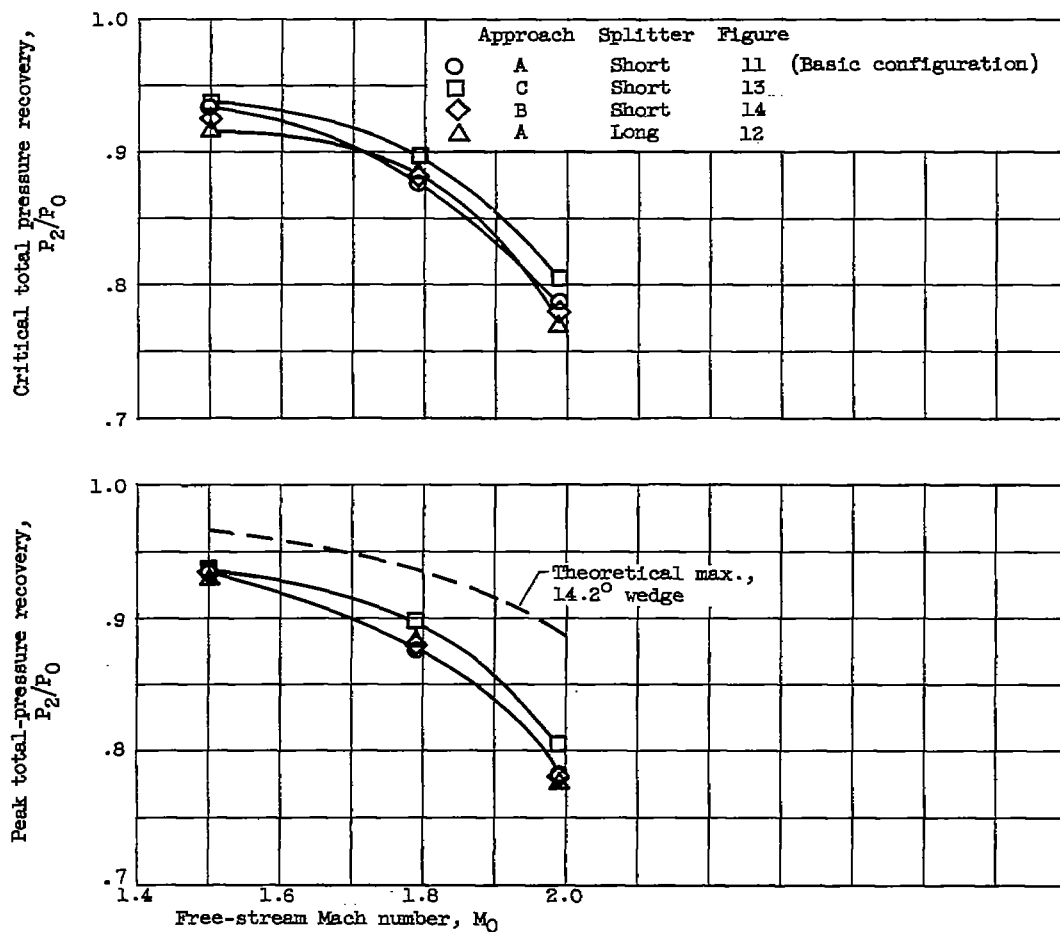
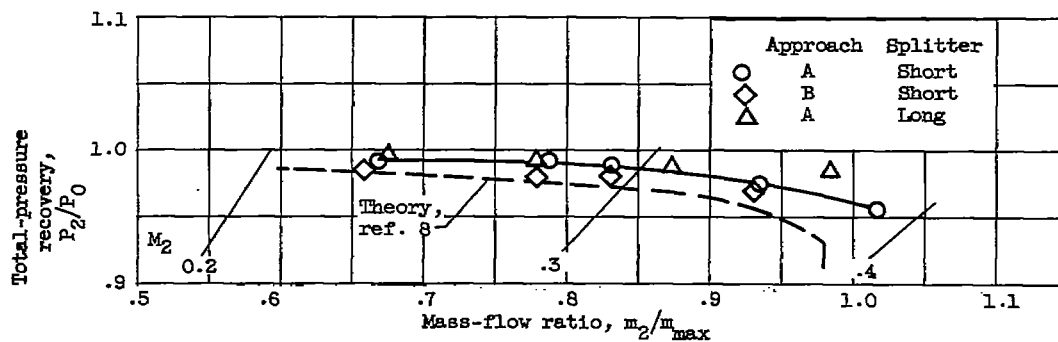


Figure 16. - Summary of total-pressure recoveries at zero angle of attack.

Figure 17. - Performance at subsonic flight speed. Free-stream Mach number, 0.63; angle of attack, 0° .

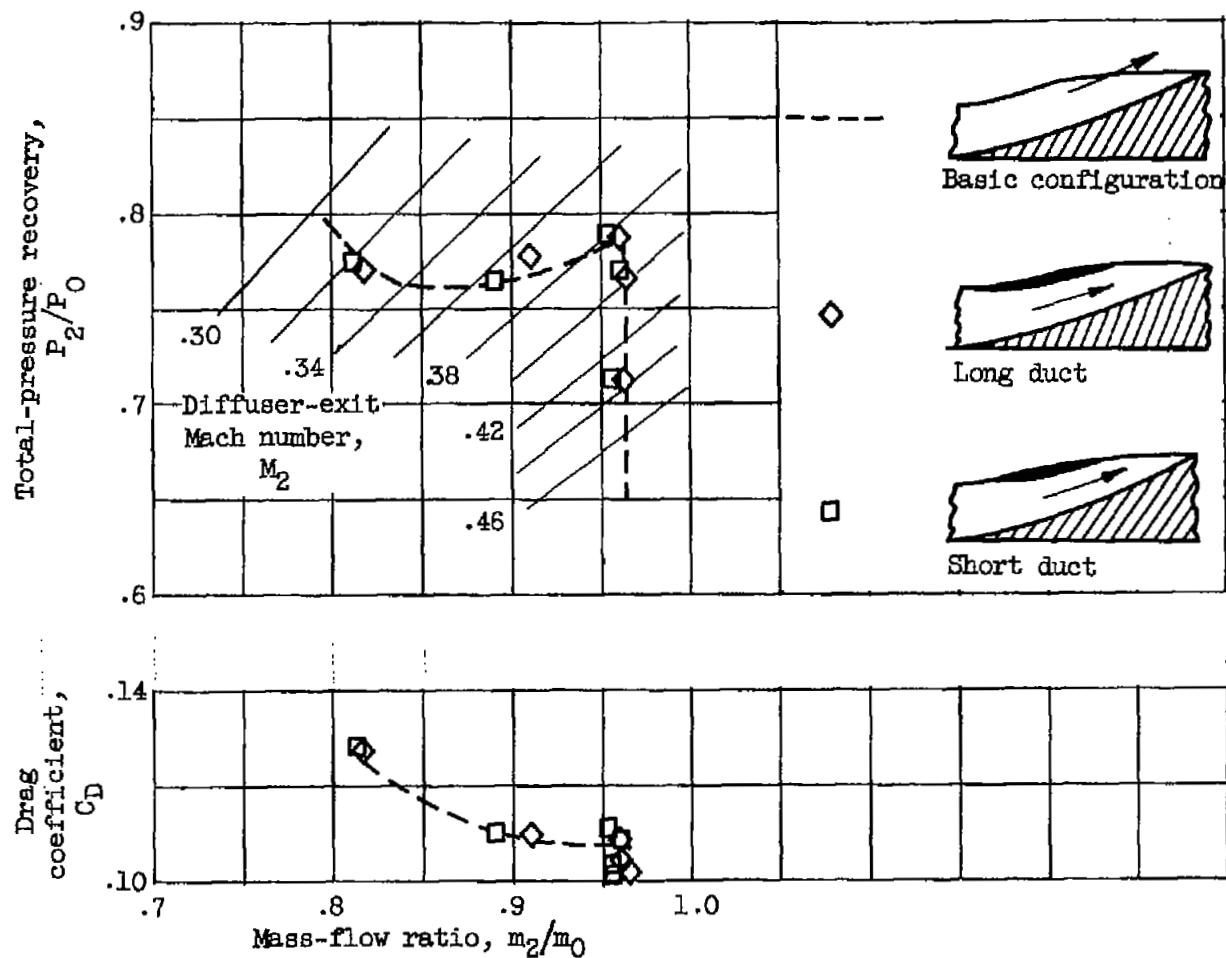
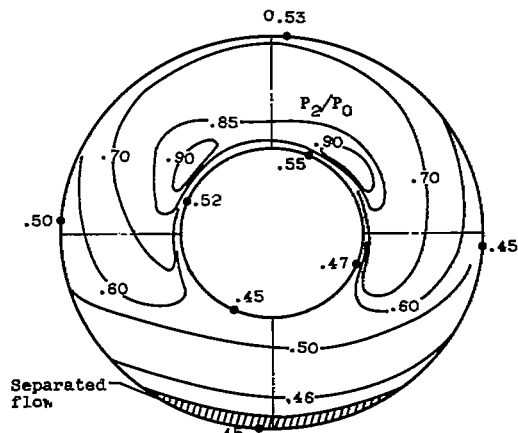
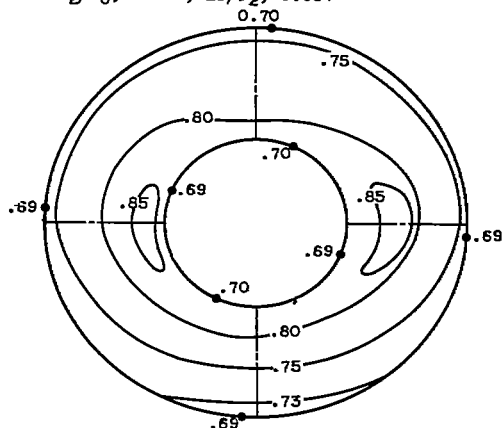


Figure 18. - Effect of enclosing boundary-layer channel. Free-stream Mach number, 1.99; angle of attack, 0° .

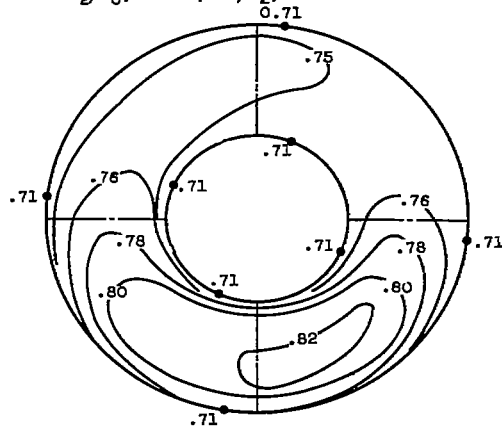
• Static pressure, P_2/P_0



(a) Supercritical mass flow; m_2/m_0 , 0.967; P_2/P_0 , 0.651; $\Delta P/P_2$, 0.68.



(b) Peak pressure recovery; m_2/m_0 , 0.958; P_2/P_0 , 0.784; $\Delta P/P_2$, 0.17.



(c) Subcritical mass flow; m_2/m_0 , 0.826; P_2/P_0 , 0.771; $\Delta P/P_2$, 0.10.

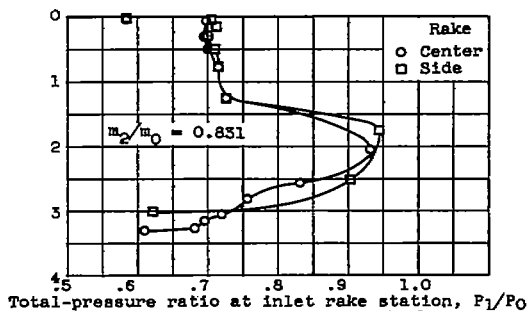
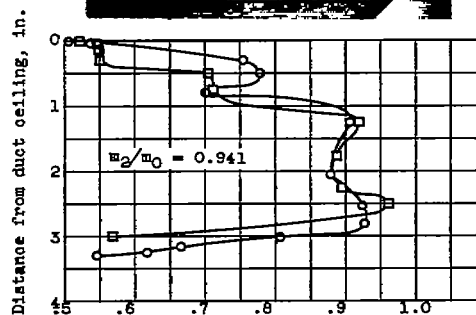
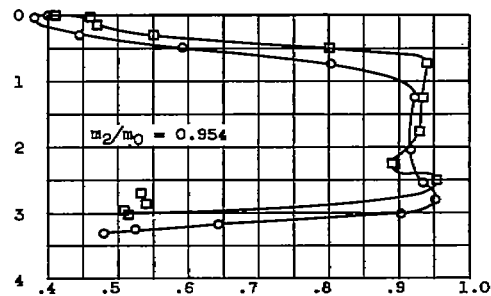
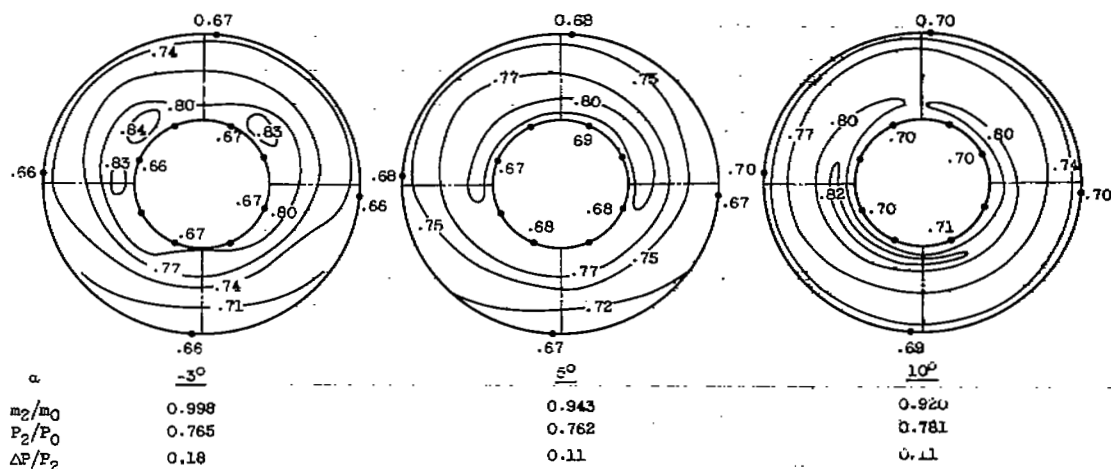


Figure 19. - Inlet and exit total-pressure distribution and corresponding shock patterns for basic configuration. Free-stream Mach number, 1.99; angle of attack, 0° .



(a) Variation with angle of attack. Free-stream Mach number, 1.99.

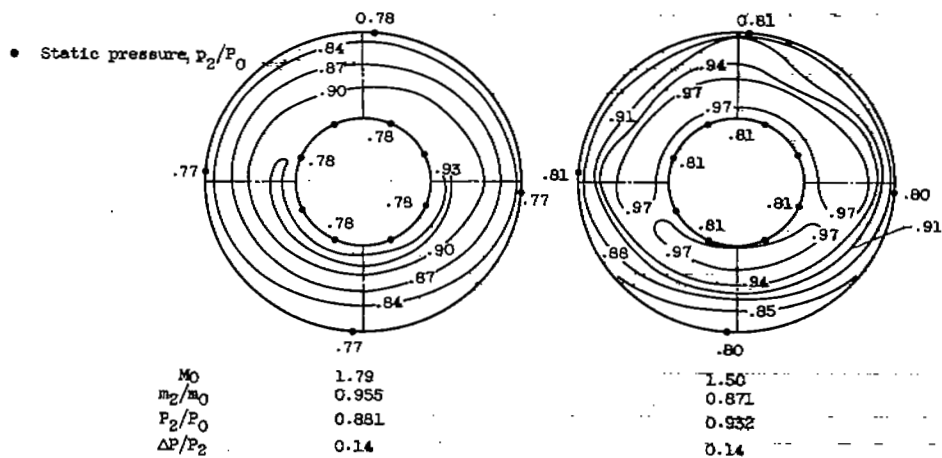
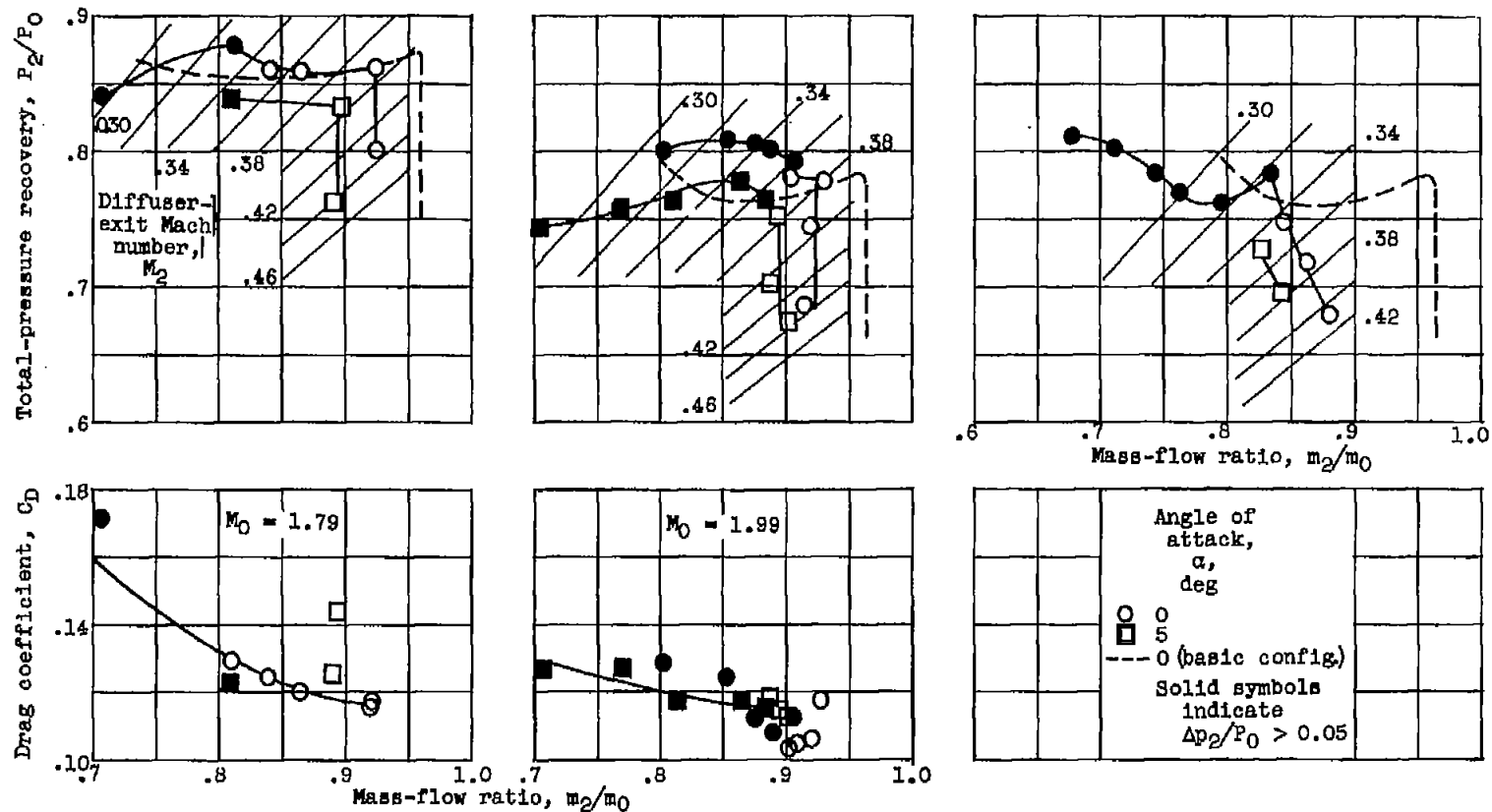
(b) Variation with Mach number. Angle of attack, 0° .

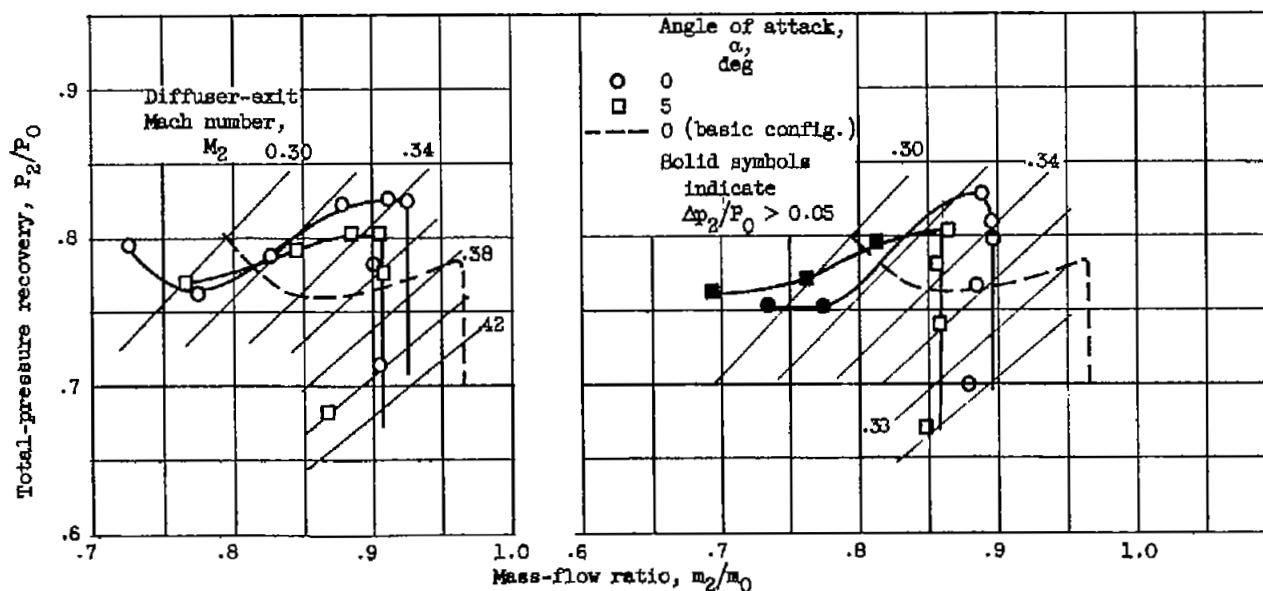
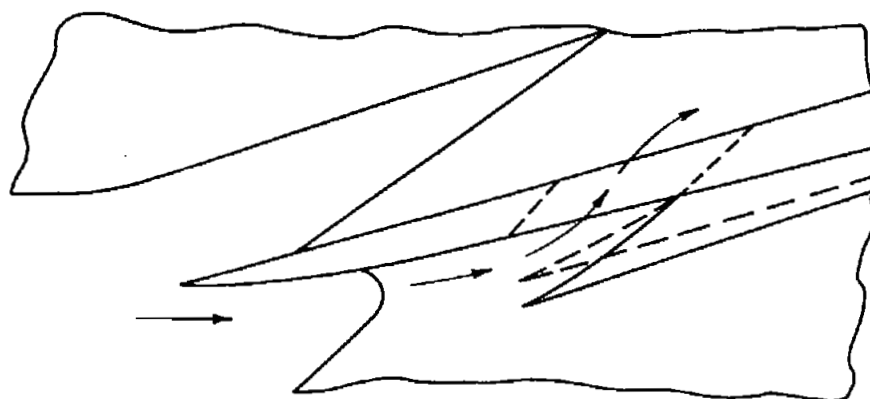
Figure 20. - Diffuser-exit total-pressure contours at critical flow for basic configuration.



(a) Flush ceiling slot.

(b) Flush ceiling slot and cowl slot.
Free-stream Mach number, 1.99.

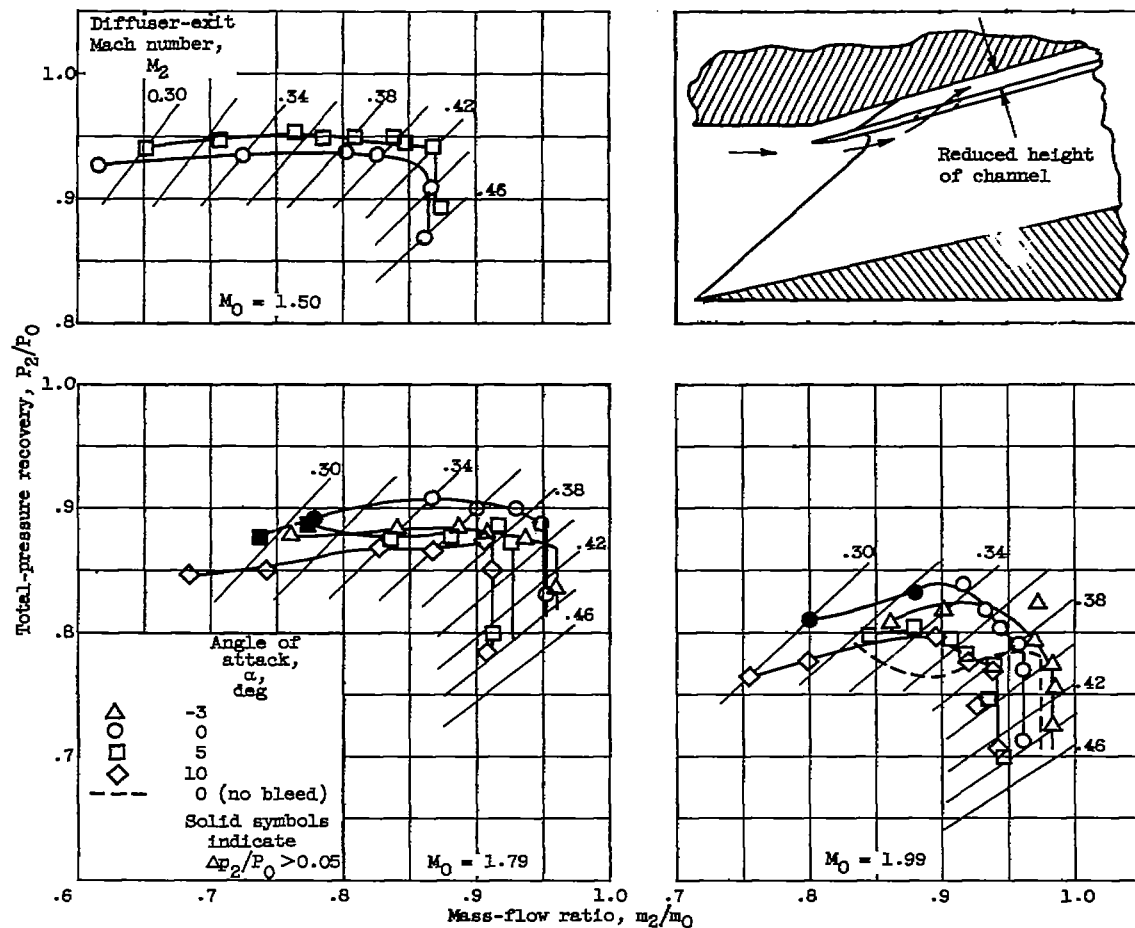
Figure 21. - Performance of throat bleeds with basic configuration.



(c) Ceiling scoop, 0.3-inch height.
Free-stream Mach number, 1.99.

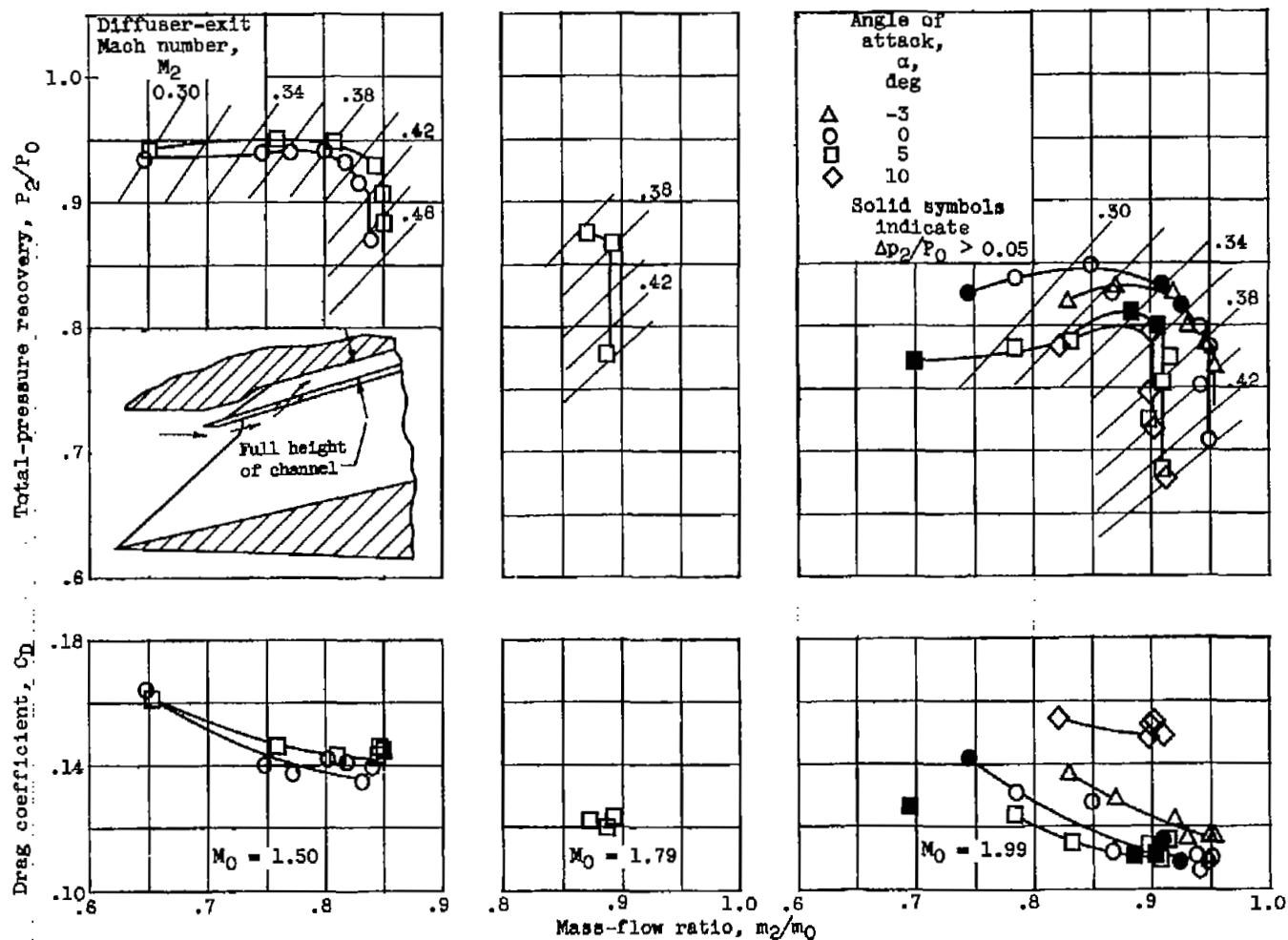
(d) Ceiling scoop, 0.5-inch height. Free-stream Mach number 1.99.

Figure 21. - Concluded. Performance of throat bleeds with basic configuration.



(a) Flush ceiling slot.

Figure 22. - Performance of throat-bleed configurations with approach B.



(b) Flush ceiling slot, full height of boundary-layer channel.

Figure 22. - Concluded. Performance of throat-bleed configurations with approach B.

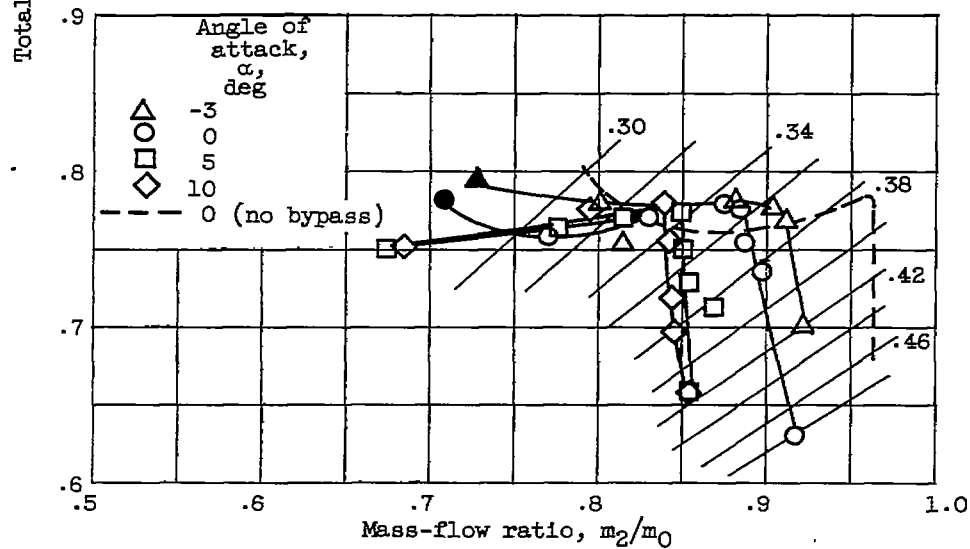
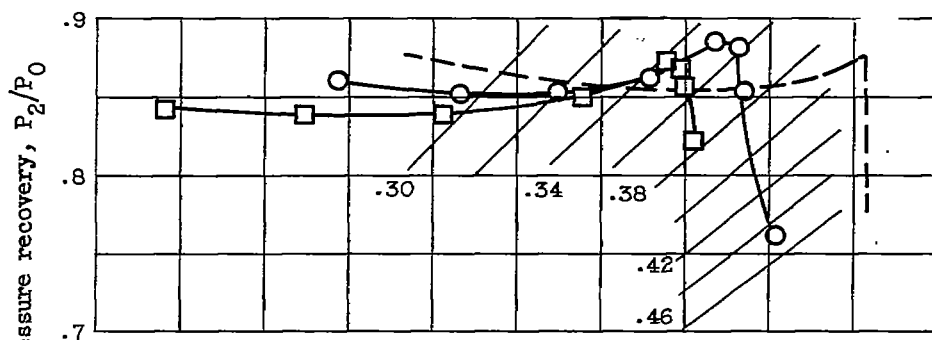
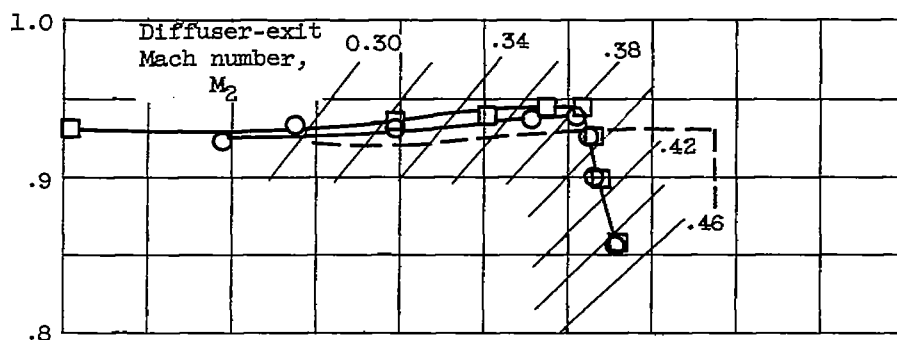


Figure 23. - Performance of basic configuration with bypass manifold.

UNCLASSIFIED

NASA Technical Library



3 1176 01436 5572

UNCLASSIFIED
CONFIDENTIAL